Supplement of Geosci. Model Dev., 17, 2471–2492, 2024
https://doi.org/10.5194/gmd-17-2471-2024-supplement

Geoscientific Model Development
Open Access

Supplement of

Intercomparison of multiple two-way coupled meteorology and air quality models (WRF v4.1.1–CMAQ v5.3.1, WRF–Chem v4.1.1, and WRF v3.7.1–CHIMERE v2020r1) in eastern China

Chao Gao et al.

Correspondence to: Xuelei Zhang (zhangxuelei@iga.ac.cn) and Aijun Xiu (xiuaijun@iga.ac.cn)

Supplement

S1. Evaluations of other meteorological variables

S1.1. Ground-based observations

For Q2, RMSEs between WRF-CMAQ, WRF-Chem, and WRF-CHIMERE simulations and surface observation were consistently below 3 g kg^{-1}, as illustrated in Table S3 and Fig. S2. Most models exhibited a tendency to underestimate annual and seasonal Q2, with MBs ranging from −0.57 to −0.18 g kg^{-1} and −1.16 to +0.20 g kg^{-1} in WRF-Chem and WRF-CHIMERE, respectively. The more obvious underestimations appeared in summer. In the MICS-Asia III project, Gao et al. (2018) reported that all the seven included two-way coupled models produced slightly positive values for Q2 during January 2010 over the North China Plain. In contrast to simulations without enabling aerosol feedbacks, the negative biases in annual and seasonal Q2 simulated by WRF-CMAQ_ARI and WRF-CHIMERE_ARI were amplified, and the WRF-CMAQ_ARI simulations exhibited bigger negative biases (see Fig. 3 and Table S3). The changes in annual, summer, and autumn MBs for WRF-Chem_ARI were consistent with the trend of WRF-CMAQ_ARI, except for spring and winter.

The annual and seasonal correlation coefficients of precipitation were 0.56–0.69, 0.46–0.63, and 0.25–0.55 for WRF-CMAQ, WRF-Chem, and WRF-CHIMERE, respectively (Table S3 and Fig. S5). All simulated results presented the highest correlations in winter and the lowest in summer and the possible reasons are due to the much more convective activities in summertime, which are not accurately captured in all coupled models. WRF-CMAQ and WRF-CHIMERE exhibited underestimation and overestimation in annual and seasonal precipitation, respectively. At the annual and seasonal scales, WRF-Chem and WRF-CHIMERE overestimated the daily precipitation magnitude by more than 1 mm day^{-1}, and WRF-CMAQ underestimated it by approximately 0.5 mm day^{-1}. A similar conclusion was obtained for North America during 2010, with the magnitude of precipitation MBs being higher in WRF-Chem compared to WRF-CMAQ (refer to Fig. 11 in Makar et al., 2015). The largest precipitation MBs simulated by the three models occurred in summer and varied from −0.70 to + 1.39 mm day^{-1}. The RMSE was highest in WRF-CHIMERE, followed by WRF-Chem, and WRF-CMAQ, and all models had the largest (> 10 mm day^{-1}) and smallest (approximately 2.5 mm day^{-1}) values in summer and winter, respectively. Considering the ARI effects, WRF-CMAQ_ARI simulations amplified the underestimations of annual and seasonal precipitation in eastern China. In contrast, WRF-Chem_ARI (except for autumn) and WRF-CHIMERE_ARI simulations mitigated the overestimations of precipitation. The effects of ARI on summer MBs were larger in all three coupled models compared to other seasons. When ACI effects were further included, WRF-Chem_BOTH demonstrated only marginal improvement in precipitation overestimation compared to WRF-Chem_NO, while WRF-CHIMERE_BOTH gave out certain enhancement of precipitation overestimation. This can be interpreted as follows: WRF-CHIMERE has the ability to simulate the activation of aerosol particles into cloud ice via heterogeneous ice nucleation and homogeneous freezing, whereas WRF-Chem lacks this capability.

Overall, the PBLH was not well simulated by any of the three coupled models, which may be a result of the adoption of low resolution sounding data in evaluations (Brunner et al., 2015) and the different settings of Richardson number thresholds in the calculation of observed PBLH (Guo et al., 2016). At 08:00 and 20:00 local time (LT), the simulated PBLHs in WRF-CMAQ have lower correlations only ranging from 0.21 to 0.40 and largest negative MBs varying from −400 to −133 m. These poor performances were mainly caused by: 1) different configurations of the PBL scheme were employed in this study, namely, WRF-CMAQ adopted the ACM2 scheme with hybrid local–nonlocal closure, while WRF-Chem and WRF-CHIMERE adopted the YSU scheme with non-local closure (Table 1); 2) Richardson number threshold was set to different values for unstable atmospheric conditions, i.e., the YSU and ACM2 schemes using the thresholds of 0 and 0.25, respectively (Xie et al., 2012); 3) different to the YSU scheme, the ACM2 scheme considers the entrainment layer in the PBLH calculations (Xie et al., 2012).

Meanwhile, all correlations of PBLH simulated by the three coupled models at 20:00 LT (R = 0.3–0.4) were better than those at 08:00 LT (R = 0.1–0.2), which indicated that the PBL schemes in these model were able to calculate PLBH after PBL collapsing a little better than before PBL developing and more observation with better spatiotemporal resolutions are needed to further evaluate the models' performance. In addition, the RMSEs of PBLH in autumn (369.89–388.79 m) and winter (347.48–392.38 m) were smaller than those in spring (405.61–622.37 m) and summer (348.80–570.16 m) for all three models.

As shown in Fig. 3 and Table S3, the changes of MB and RMSE of simulated PBLH induced by the effects of aerosol feedbacks were greater than those of R. Meanwhile, the MBs were further analyzed. For WRF-CMAQ, ARI effects induced an increase (−1.93 m) and decrease (+6.66 m) in the annual underestimations of PBLH at 8:00 and 20:00 LT, respectively (Table S3). The negative MBs for WRF-Chem_ARI and WRF-Chem_BOTH showed an enhancement (08:00 LT: −25.25 m, 20:00 LT: −25.60 m) and reduction (08:00 LT: +19.65 m, 20:00 LT: +14.09 m) compared to those for WRF-Chem_NO and WRF-Chem_ARI, respectively. Both the ARI (−6.17 and −3.34 m) and ACI (−0.65 and −1.11 m) effects further underestimated annual PBLH at 08:00 and 20:00 LT for WRF-CHIMERE. Note that the variations in MBs induced by aerosol feedbacks for the three coupled models at the annual scale were similar to those at the seasonal scale.

S1.2. Satellite-borne observations

As indicated in Table 3, the three coupled models demonstrated good performance in simulating the shortwave radiation at *the* top of the atmosphere (SRTOA) and longwave radiation at *the* top of the atmosphere (LRTOA). The annual MBs for SRTOA and LRTOA are ranging from −4.40 to +5.42 W m^{-2} and −2.14 to 0.66 W m^{-2}, respectively. Seasonal SRTOA was also well simulated by all three models, especially in winter (Figure S10). For seasonal LRTOA, the WRF-CMAQ and WRF-Chem model performances were better than that of WRF-CHIMERE for all seasons except autumn (Figure S11). No matter whether ARI and/or ACI effects were enabled or not, simulations by WRF-CMAQ exhibited negative MBs in all seasons and WRF-

CHIMERE displayed negative MBs in all seasons except for spring. For WRF-Chem, it produced underestimations and overestimations of SRTOA in spring–summer and autumn–winter, respectively.

S2. Evaluations of other air quality variables

According to the annual statistical results (Table 4 and Fig. S17), the NO_2 simulated by all three models had comparable correlations (0.50–0.60) with ground-based observations. WRF-CMAQ slightly overestimated NO_2 (MBs of +2.74 to +3.26 μg m^{-3}, and NMBs of +8.77% to +10.44%). In contrast, WRF-Chem (MBs of −10.03 to −9.22 μg m^{-3}, and NMBs of −32.14% to −29.55%) and WRF-CHIMERE (MBs of −9.35 to −8.96 μg m^{-3}, and NMBs of −29.96% to −28.73%) tended to significantly underestimate NO_2 in eastern China. For seasonal variations (Fig. 7), WRF-CMAQ showed the best performance in winter, and generally overestimated NO_2 in all seasons with the NMBs ranging from −2.21% to 34.34%. Both WRF-Chem and WRF-CHIMERE had maximum R and NMB values (0.42 to 0.50 and −13.09% to −3.23%, respectively) in winter, and minimum values (0.57 to 0.62 and −41.57% to −38.05%, respectively) in summer. The annual and seasonal positive biases of WRF-CMAQ are partially caused by lack of incorporation of heterogeneous reactions of NO_2 that occurred on ground and aerosol surfaces (Spataro et al., 2013; Li et al., 2018; Liu et al., 2019). Recently, Zhang et al. (2021) addressed these gaps in CMAQ v5.3 but related modules had not been integrated into the latest officially released version (version 5.4). For WRF-Chem and WRF-CHIMERE, underestimations of NO_2 were consistent with overestimations of O_3, as the NO_x depletions were dominated by O_3 titrations. In addition, subtle differences existed in the default settings of reaction rate constants for specific chemical reactions referring to NO_x in WRF-CMAQ, WRF-Chem, and WRF-CHIMERE. More detailed information can be found in the source code files of mech_cb6r3_ae6_aq.def, module_cbmz.F, and rates.F, respectively. With ARI feedbacks enabled, the annual and seasonal R values of NO_2 simulated by WRF-CMAQ improved, but the NMBs worsened. In contrast, both WRF-Chem and WRF-CHIMERE presented improvements. Our results showed that ARI effects tended to amplify NO_2 overestimations in WRF-CMAQ, and alleviate underestimations in WRF-Chem and WRF-CHIMERE. This can be explained by the ARI-induced NO_2 reductions being associated with slower photochemical reactions, strengthened atmospheric stability and O_3 titration, and vice versa. The inclusion of ACI effects in WRF-Chem and WRF-CHIMERE resulted in relatively limited improvements in model performances.

All models had the poorest performance in the annual and seasonal SO_2 and CO simulations over eastern China (Table 4 and Fig. 6). For SO_2, annual correlations were comparable for all models ranging from 0.39 to 0.41. All three models underestimated SO_2. WRF-CMAQ showed the smallest MB of −4.31 μg m^{-3}, while WRF-Chem had the largest of −10.30 μg m^{-3}. Gao et al. (2018) also demonstrated that all two-way coupled models, except the WRF-Chem version from the University of Iowa *modelling* group, tended to underestimate SO_2 (−54.77 to 4.50 μg m^{-3}) over the North China Plain during January 2013. The R values for all models were highest in autumn and winter (0.31–0.46) and lowest in spring and summer (0.16–0.38), while NMBs showed the opposite trend. As concluded by Liu et al. (2010), the larger underestimations of seasonal SO_2 concentrations were caused by the weaker solar radiation and lower amount of precipitation in winter compared to summer. These conditions slowed down the photochemical conversion of SO_2 to SO_4^{2-}, wet scavenging, and aqueous-phase oxidation rates of SO_2.

For CO (Table 4), WRF-CHIMERE (0.47–0.48) had higher correlation coefficients than those of WRF-CMAQ (0.23–0.24) and WRF-Chem (0.21–0.22). All three models underestimated CO concentrations, with MBs ranging from −0.52 to −0.39 mg m^{-3}. These underestimations were partly attributed to uncertainties in the vertical allocation of CO emissions (He et al., 2017). WRF-CMAQ and WRF-Chem both produced spring-minimum (0.15) and winter-maximum (0.36) seasonal cycles of R values (Fig. 6), while WRF-CHIMERE presented high (0.47) and low (0.26) correlations in winter and summer, respectively. Negative seasonal NMBs varied from −56.94% to −33.18% in all coupled models. When ARI effects were considered, annual and seasonal SO_2 and CO model performances in all three models showed slight improvement (R increased approximately 0.01 and NMB enhanced from 0.98% to 1.71%). Moreover, the enhancements in the simulation accuracies of SO_2 and CO for the two-way coupled WRF-Chem and WRF-CHIMERE were dominated by ARI effects rather than ACI effects.

S3. Statistical metrics

The correlation coefficient (R), mean bias (MB), normalized mean bias (NMB), normalized gross error (NGE) and root mean square error (RMSE) were adopted to assess the accuracy of coupled models in simulating meteorological and air quality parameters against the ground-based and satellite observations with the following equations:

$$R=\frac{\sum_{i=1}^{N}(p_i-\bar{p})(o_i-\bar{o})}{\sqrt{\sum_{i=1}^{N}(p_i-\bar{p})^2}\sqrt{\sum_{i=1}^{N}(o_i-\bar{o})^2}} \quad (S1)$$

$$MB=\frac{1}{N}\sum_{i=1}^{N}(p_i-o_i) \quad (S2)$$

$$NMB=\frac{\sum_{i=1}^{N}(p_i-o_i)}{\sum_{i=1}^{N}(o_i)} \quad (S3)$$

$$NGE=\frac{\sum_{i=1}^{N}|p_i-o_i|}{\sum_{i=1}^{N}(o_i)} \quad (S4)$$

$$RMSE=\left[\frac{1}{N}\sum_{i=1}^{N}(p_i-o_i)^2\right]^{1/2} \quad (S5)$$

where p_i and o_i are the simulated and observed parameters, respectively, n is the total number of the values used for evaluation, and $\bar{p}$ and $\bar{o}$ are the averages of the simulation and observation, respectively.

Table S1. Summary of representations of cloud cover and cloud optical properties in the Fast-JX scheme for WRF-CMAQ, WRF-Chem and WRF-CHIMERE.

Model	Cloud clover	Cloud optical properties			
		Optical properties	Effective Wavelength	Hydrometeor types	Method
WRF-CMAQ	1. CF[a] from WRF and CF calculated using RH and RH thresholds 2. Exponential-random overlapping	Extinction, single scattering albedo and asymmetry factor	294.6, 303.2, 310.0, 316.4, 333.1, 382.0 and 607.7 nm	Cloud liquid water, rain, snow, graupel and ice	The parameterizations proposed by Hu and Stamnes (1993) and Fu (1996)
WRF-Chem	1. CF=0 if CLWC[b]=0 2. CF=1 if CIC[c]>0	Cloud optical depth	300, 400, 600 and 999 nm	Cloud liquid water	Based on the empirical functions of relative humidity and cloud liquid water content
WRF-CHIMERE	1. CF=0 if CLWC or CIWC=0 2. CF=1 if CLWC or CIC>0	Cloud optical depth	200, 300, 400, 600, and 999 nm	Cloud liquid water and ice	Based on the functions of cloud effective *radii* and cloud liquid water/ice content

[a]CF is cloud fraction. [b]CLWC is cloud liquid water content. [c]CIC is cloud ice content.

Table S2. Summary of the treatments for aerosol size distributions and components in each mode or bin for the coupled WRF-CMAQ, WRF-Chem and WRF-CHIMERE models.

Model	Aerosol mechanism	Modal approach									
		Aitken				Accumulation		Coarse			
WRF-CMAQ	AERO6	BC, OC, sulfate, nitrate, ammonium, PMOTHR[d], PNCOM[e] water, metals				BC, OC, sulfate, nitrate, ammonium, PMOTHR, PNCOM, water, metals, sea salt, dust		PMC[f], sea salt, dust			
		Sectional approach									
WRF-Chem	MOSAIC[a]	Bin 1		Bin 2		Bin 3		Bin 4			
		0.039–0.156 μm		0.156–0.625 μm		0.625–2.5 μm		2.5–10.0 μm			
		Black carbon (BC), OC, sulfate, nitrate, sea salt[d]		BC, OC, sulfate, nitrate, sea salt		BC, OC, sulfate, nitrate, sea salt		*Dust*, sea salt, OIN[g]			
WRF-CHIMERE	SAM[b]	Bin 1	Bin 2	Bin 3	Bin 4	Bin 5	Bin 6	Bin 7	Bin 8	Bin 9	Bin 10
		0.039–0.078 μm	0.078–0.156 μm	0.156–0.312 μm	0.312–0.625 μm	0.625–1.25 μm	1.25–2.5 μm	2.5–5.0 μm	5.0–10.0 μm	10.0–20.0 μm	20.0–40
		BC, OC, sulfate, PPM[c]	BC, OC, sulfate, PPM	BC, OC, sulfate, PPM	BC, OC, sulfate, PPM	BC, OC, sulfate, PPM	BC, OC, sulfate, dust, sea salt	Dust, sea salt	BC, OC, PPM, dust, sea salt	Dust, sea salt	Dust

[a]MOSAIC is the Model for Simulating Aerosol Interactions and Chemistry, and the cbmz-mosaic emissions in "PNNL" format (emiss_inpt_opt==101) was used in WRF-Chem simulations.
[b]SAM is the sectional aerosol mechanism.
[c]PPM is the primary particulate matter.
[d]PMOTHR is the remaining particulate matter that *can not be speciated into* fine mode, and more detailed information is at https://www.airqualitymodeling.org/index.php/CMAQv5.0_PM_emitted_species_list.
[e]PNCOM is the primary non-carbon organic matter in fine mode and more detailed information is at https://www.airqualitymodeling.org/index.php/CMAQv5.0_PM_emitted_species_list.
[f]PMC is the primary particulate matter in coarse mode and more detailed information is at https://www.airqualitymodeling.org/index.php/CMAQv5.0_PM_emitted_species_list.
[g]OIN is the other inorganic matter.

Table S3. Statistical metrics (R, MB, NMB, *NGE*, and RMSE) between simulated and observed annual SSR, T2, RH2, Q2, WS10, WD10, precipitation, and PBLH at 08:00 and 20:00 LT) in eastern China. The best results are in bold, while mean simulations and observations are in italics.

Variables	Statistics	WRF-CMAQ_NO	WRF-CMAQ_ARI	WRF-Chem_NO	WRF-Chem_ARI	WRF-Chem_BOTH	WRF-CHIMERE_NO	WRF-CHIMERE_ARI	WRF-CHIMERE_BOTH
SSR (*155.22* W m^{-2})	Mean_sim	*191.12*	*171.14*	*194.52*	*180.04*	*191.71*	*197.88*	*188.63*	*189.54*
	R	0.88	**0.89**	0.88	**0.89**	0.88	0.85	0.85	0.85
	MB	35.89	15.91	39.30	24.82	36.48	42.65	33.41	34.32
	NMB (%)	23.12	**10.25**	25.32	15.99	23.50	27.48	21.52	22.11
	NGE (%)	206.62	170.85	202.41	**170.70**	208.05	242.53	221.67	226.29
	RMSE	133.05	**120.60**	134.16	123.94	134.45	154.71	147.73	148.57
T2	Mean_sim	*12.81*	*12.61*	*12.99*	*12.84*	*12.96*	*11.84*	*11.68*	*11.69*
(*13.68* °C)	R	**0.97**	**0.97**	**0.97**	**0.97**	**0.97**	0.96	0.96	0.96

	MB	-0.86	-1.06	-0.68	-0.83	-0.71	-1.83	-2.00	-1.98
	NMB (%)	-6.33	-7.76	**-4.97**	-6.09	-5.21	-13.39	-14.60	-14.50
	NGE (%)	**10.58**	10.76	10.79	10.95	10.86	17.00	17.65	17.60
	RMSE	**2.88**	2.94	3.05	3.07	3.05	3.87	3.94	3.97
Q2	Mean_sim	*8.69*	*8.51*	*8.57*	*8.54*	*8.58*	*8.35*	*8.30*	*8.30*
(*8.87* g kg^{-1})	R	**0.90**	**0.90**	0.89	0.89	0.89	0.88	0.88	0.88
	MB	-0.18	-0.35	-0.30	-0.32	-0.28	-0.52	-0.57	-0.56
	NMB (%)	**-2.00**	-3.98	-3.36	-3.66	-3.19	-5.84	-6.37	-6.35
	NGE (%)	**16.80**	16.85	19.70	19.66	19.77	20.55	20.65	20.62
	RMSE	**2.93**	2.95	3.09	3.09	3.10	3.17	3.18	3.18
RH2	Mean_sim	*71.03*	*70.51*	*70.01*	*70.33*	*70.13*	*70.41*	*70.58*	*70.46*
(*67.48* %)	R	**0.73**	**0.73**	0.68	0.68	0.68	0.65	0.65	0.65
	MB	3.55	3.03	2.53	2.85	2.64	2.93	3.10	2.97
	NMB (%)	5.26	4.49	**3.74**	4.22	3.92	4.34	4.59	4.41
	NGE (%)	**19.90**	19.91	23.45	23.71	23.71	24.77	24.88	24.90
	RMSE	**18.92**	18.98	19.78	19.79	19.84	20.81	20.82	20.84
WS10	Mean_sim	*3.27*	*3.23*	*3.30*	*3.29*	*3.30*	*3.85*	*3.83*	*3.83*
(*2.81* m s^{-1})	R	**0.62**	0.61	0.60	0.59	0.59	0.47	0.47	0.47
	MB	0.45	0.42	0.49	0.48	0.49	1.04	1.02	1.02
	NMB (%)	16.16	**14.98**	17.45	17.11	17.53	36.98	36.27	36.34
	NGE (%)	96.20	**95.00**	100.16	100.09	100.55	136.55	135.59	135.75
	RMSE	1.89	1.88	1.92	1.92	1.93	2.46	2.45	2.45
WD10 (*175.27* °)	Mean_sim	*177.13*	*176.62*	*177.87*	*177.82*	*178.11*	*171.97*	*171.53*	*171.68*
	R	0.01	0.01	0.01	0.01	0.01	0.02	0.02	0.02
	MB	1.85	1.35	2.60	2.55	2.83	-3.31	-3.74	-3.60
	NMB (%)	1.06	0.77	1.48	1.45	1.62	-1.89	-2.14	-2.05
	NGE (%)	94.30	**94.00**	101.16	101.09	101.55	126.75	125.79	125.85
	RMSE	149.57	149.45	149.45	149.38	149.57	148.70	148.47	148.71
Precipitation	Mean_sim	*2.46*	*2.31*	*3.24*	*3.19*	*3.26*	*3.31*	*3.24*	*3.21*
(PREC)	R	**0.59**	**0.59**	0.50	0.50	0.50	0.35	0.34	0.34
(*2.72* mm d^{-1})	MB	-0.27	-0.42	0.51	0.46	0.53	0.59	0.52	0.48
	NMB (%)	**-9.80**	-15.35	18.86	16.83	19.43	21.46	18.96	17.63
	NGE (%)	310.71	**283.10**	442.60	428.11	445.89	573.24	565.36	557.56
	RMSE	8.03	**7.96**	10.32	10.26	10.33	10.87	10.85	10.93
PBLH00	Mean_sim	*253.54*	*251.61*	*288.41*	*263.16*	*282.81*	*276.45*	*270.28*	*269.63*
(*432.13* m)	R	**0.21**	**0.21**	0.17	0.17	0.17	0.17	0.17	0.17
	MB	-178.59	-180.52	-143.72	-168.97	-149.32	-155.68	-161.85	-162.50
	NMB (%)	-41.33	-41.77	**-33.26**	-39.10	-34.55	-36.03	-37.45	-37.61
	NGE (%)	58.89	58.75	**54.37**	56.96	54.51	57.20	57.63	57.28
	RMSE	380.23	378.79	**371.27**	379.72	372.14	373.78	375.85	374.52
PBLH12	Mean_sim	*230.14*	*236.80*	*358.05*	*332.45*	*346.54*	*363.47*	*360.13*	*359.03*
(*547.02* m)	R	**0.40**	**0.40**	0.39	**0.40**	0.39	0.34	0.35	0.35
	MB	-316.88	-310.22	-188.97	-214.57	-200.48	-183.55	-186.89	-188.00
	NMB (%)	-57.93	-56.71	-34.55	-39.22	-36.65	**-33.56**	-34.16	-34.37

NGE (%)	65.84	65.23	59.55	59.05	59.49	59.65	**59.32**	59.66
RMSE	505.64	502.24	459.64	460.51	**459.50**	470.39	467.90	469.19

Table S4. Effects of aerosol feedbacks (ARI and/or ACI) considered in different coupled models on *statistical* metrics between annual and seasonal meteorological and air quality simulations and observations in eastern China.

Surface observations		WRF-CMAQ_ARI	WRF-Chem_ARI	WRF-Chem_ACI	WRF-Chem_BOTH	WRF-CHIMERE_ARI	WRF-CHIMERE_ACI	WRF-CHIMERE_BOTH
SSR	Annual	R(↑), MB(↓), RMSE(↓)	R(↑), MB(↓), RMSE(↓)	R(↓), MB(↑), RMSE(↑)	R(↑), MB(↓), RMSE(↓)	R(↑), MB(↓), RMSE(↓)	R(↓), MB(↑), RMSE(↑)	R(↑), MB(↓), RMSE(↓)
	Spring	R(↑), MB(↓), RMSE(↓)	R(↑), MB(↓), RMSE(↓)	R(↓), MB(↑), RMSE(↑)	R(↓), MB(↓), RMSE(↓)	R(↑), MB(↓), RMSE(↓)	R(↓), MB(↓), RMSE(↑)	R(↑), MB(↓), RMSE(↓)
	Summer	R(↑), MB(↓), RMSE(↓)	R(↑), MB(↓), RMSE(↓)	R(↓), MB(↑), RMSE(↑)	R(↑), MB(↓), RMSE(↓)	R(↑), MB(↓), RMSE(↓)	R(↑), MB(↑), RMSE(↓)	R(↑), MB(↓), RMSE(↓)
	Autumn	R(↑), MB(↓), RMSE(↓)	R(↑), MB(↓), RMSE(↓)	R(↓), MB(↑), RMSE(↑)	R(↓), MB(↓), RMSE(↓)	R(↑), MB(↓), RMSE(↓)	R(↓), MB(↑), RMSE(↑)	R(↑), MB(↓), RMSE(↓)
	Winter	R(↑), MB(↓), RMSE(↓)	R(↑), MB(↓), RMSE(↓)	R(↓), MB(↑), RMSE(↑)	R(↑), MB(↓), RMSE(↓)	R(↑), MB(↓), RMSE(↓)	R(↓), MB(↓), RMSE(↑)	R(↑), MB(↓), RMSE(↓)
T2	Annual	R(↓), MB(↓), RMSE(↑)	R(↑), MB(↓), RMSE(↑)	R(↓), MB(↑), RMSE(↓)	R(↑), MB(↓), RMSE(↑)	R(↑), MB(↓), RMSE(↑)	R(↓), MB(↑), RMSE(↑)	R(↓), MB(↓), RMSE(↑)
	Spring	R(↓), MB(↓), RMSE(↑)	R(↑), MB(↓), RMSE(↑)	R(↓), MB(↑), RMSE(↓)	R(↑), MB(↓), RMSE(↑)	R(↑), MB(↓), RMSE(↑)	R(↓), MB(↓), RMSE(↑)	R(↓), MB(↓), RMSE(↑)
	Summer	R(↓), MB(↓), RMSE(↑)	R(↑), MB(↓), RMSE(↓)	R(↓), MB(↑), RMSE(↓)	R(↑), MB(↑), RMSE(↓)	R(↓), MB(↓), RMSE(↑)	R(↑), MB(↑), RMSE(↓)	R(↑), MB(↓), RMSE(↑)
	Autumn	R(↓), MB(↓), RMSE(↑)	R(↑), MB(↓), RMSE(↑)	R(↓), MB(↑), RMSE(↓)	R(↑), MB(↓), RMSE(↓)	R(↑), MB(↓), RMSE(↑)	R(↓), MB(↑), RMSE(↓)	R(↓), MB(↓), RMSE(↑)
	Winter	R(↑), MB(↓), RMSE(↑)	R(↑), MB(↓), RMSE(↑)	R(↑), MB(↑), RMSE(↓)	R(↑), MB(↓), RMSE(↑)	R(↑), MB(↓), RMSE(↑)	R(↓), MB(↓), RMSE(↑)	R(↑), MB(↓), RMSE(↑)
SH2	Annual	R(↓), MB(↓), RMSE(↑)	R(↑), MB(↓), RMSE(↓)	R(↓), MB(↑), RMSE(↑)	R(↓), MB(↑), RMSE(↑)	R(↓), MB(↓), RMSE(↑)	R(↓), MB(↑), RMSE(↑)	R(↓), MB(↓), RMSE(↑)
	Spring	R(↓), MB(↓), RMSE(↑)	R(↑), MB(↓), RMSE(↑)	R(↓), MB(↑), RMSE(↑)	R(↓), MB(↑), RMSE(↑)	R(↑), MB(↓), RMSE(↑)	R(↓), MB(↑), RMSE(↓)	R(↓), MB(↓), RMSE(↑)
	Summer	R(↓), MB(↓), RMSE(↑)	R(↑), MB(↓), RMSE(↑)	R(↓), MB(↑), RMSE(↑)	R(↓), MB(↑), RMSE(↑)	R(↓), MB(↓), RMSE(↑)	R(↓), MB(↓), RMSE(↑)	R(↓), MB(↓), RMSE(↑)
	Autumn	R(↓), MB(↓), RMSE(↑)	R(↑), MB(↓), RMSE(↑)	R(↓), MB(↑), RMSE(↓)	R(↓), MB(↑), RMSE(↓)	R(↑), MB(↓), RMSE(↑)	R(↓), MB(↑), RMSE(↓)	R(↑), MB(↑), RMSE(↑)
	Winter	R(↓), MB(↓), RMSE(↑)	R(↓), MB(↓), RMSE(↑)	R(↑), MB(↑), RMSE(↑)	R(↓), MB(↓), RMSE(↑)	R(↓), MB(↓), RMSE(↑)	R(↓), MB(↓), RMSE(↑)	R(↓), MB(↓), RMSE(↑)
Q2	Annual	R(↓), MB(↓), RMSE(↑)	R(↓), MB(↑), RMSE(↑)	R(↓), MB(↓), RMSE(↑)	R(↓), MB(↑), RMSE(↑)	R(↓), MB(↑), RMSE(↑)	R(↓), MB(↓), RMSE(↑)	R(↓), MB(↑), RMSE(↑)
	Spring	R(↓), MB(↓), RMSE(↑)	R(↓), MB(↑), RMSE(↑)	R(↓), MB(↓), RMSE(↑)	R(↓), MB(↑), RMSE(↑)	R(↓), MB(↑), RMSE(↑)	R(↓), MB(↑), RMSE(↑)	R(↓), MB(↑), RMSE(↑)
	Summer	R(↓), MB(↓), RMSE(↑)	R(↓), MB(↑), RMSE(↓)	R(↓), MB(↓), RMSE(↑)	R(↑), MB(↓), RMSE(↓)	R(↓), MB(↑), RMSE(↑)	R(↑), MB(↓), RMSE(↓)	R(↓), MB(↓), RMSE(↓)
	Autumn	R(↓), MB(↓), RMSE(↑)	R(↓), MB(↑), RMSE(-)	R(↓), MB(↓), RMSE(↑)	R(↓), MB(↑), RMSE(↑)	R(↑), MB(↑), RMSE(↓)	R(↓), MB(↓), RMSE(↑)	R(↓), MB(↓), RMSE(↑)
	Winter	R(↓), MB(↓), RMSE(-)	R(↑), MB(↑), RMSE(↑)	R(↓), MB(↓), RMSE(↓)	R(↓), MB(↑), RMSE(↑)	R(↑), MB(↑), RMSE(↓)	R(↓), MB(↓), RMSE(↑)	R(↑), MB(↑), RMSE(↑)
WS10	Annual	R(↓), MB(↓), RMSE(↓)	R(↓), MB(↓), RMSE(↓)	R(↓), MB(↑), RMSE(↑)	R(↓), MB(↓), RMSE(↑)	R(↓), MB(↓), RMSE(↓)	R(↑), MB(↑), RMSE(↑)	R(↓), MB(↓), RMSE(↓)
	Spring	R(↓), MB(↓), RMSE(↓)	R(↓), MB(↓), RMSE(↑)	R(↓), MB(↑), RMSE(↓)	R(↓), MB(↓), RMSE(↑)	R(↑), MB(↓), RMSE(↓)	R(↓), MB(↓), RMSE(↑)	R(↓), MB(↓), RMSE(↑)
	Summer	R(↓), MB(↓), RMSE(↑)	R(↑), MB(↓), RMSE(↓)	R(↓), MB(↑), RMSE(↑)	R(↑), MB(↑), RMSE(↑)	R(↓), MB(↓), RMSE(↑)	R(↑), MB(↓), RMSE(↓)	R(↑), MB(↓), RMSE(↓)
	Autumn	R(↓), MB(↓), RMSE(↓)	R(↓), MB(↓), RMSE(↑)	R(↓), MB(↑), RMSE(↑)	R(↓), MB(↓), RMSE(↑)	R(↑), MB(↓), RMSE(↓)	R(↓), MB(↑), RMSE(↑)	R(↓), MB(↓), RMSE(↑)
	Winter	R(↑), MB(↓), RMSE(↓)	R(↓), MB(↓), RMSE(↑)	R(↑), MB(↑), RMSE(↑)	R(↓), MB(↓), RMSE(↑)	R(↑), MB(↓), RMSE(↓)	R(↓), MB(↑), RMSE(↑)	R(↓), MB(↓), RMSE(↓)

PBLH_00	Annual	R(↑), MB(↓), RMSE(↓)	R(↑), MB(↓), RMSE(↑)	R(↓), MB(↑), RMSE(↓)	R(↑), MB(↓), RMSE(↑)	R(↓), MB(↓), RMSE(↑)	R(↑), MB(↓), RMSE(↓)	R(↑), MB(↓), RMSE(↑)
	Spring	R(↓), MB(↓), RMSE(↓)	R(↑), MB(↓), RMSE(↑)	R(↓), MB(↑), RMSE(↓)	R(↓), MB(↓), RMSE(↑)	R(↑), MB(↓), RMSE(↑)	R(↓), MB(↓), RMSE(↓)	R(↑), MB(↓), RMSE(↑)
	Summer	R(↑), MB(↓), RMSE(↓)	R(↑), MB(↓), RMSE(↑)	R(↓), MB(↑), RMSE(↓)	R(↑), MB(↓), RMSE(↓)	R(↓), MB(↓), RMSE(↑)	R(↑), MB(↑), RMSE(↓)	R(↓), MB(↓), RMSE(↑)
	Autumn	R(↑), MB(↑), RMSE(↓)	R(↑), MB(↓), RMSE(↑)	R(↑), MB(↑), RMSE(↓)	R(↑), MB(↓), RMSE(↑)	R(↑), MB(↓), RMSE(↑)	R(↑), MB(↓), RMSE(↓)	R(↑), MB(↓), RMSE(↑)
	Winter	R(↓), MB(↑), RMSE(↓)	R(↓), MB(↓), RMSE(↑)	R(↑), MB(↑), RMSE(↓)	R(↑), MB(↓), RMSE(↑)	R(↓), MB(↑), RMSE(↓)	R(↑), MB(↑), RMSE(↓)	R(↑), MB(↑), RMSE(↓)
PBLH_12	Annual	R(↑), MB(↑), RMSE(↓)	R(↑), MB(↓), RMSE(↑)	R(↓), MB(↑), RMSE(↓)	R(↓), MB(↓), RMSE(↓)	R(↑), MB(↓), RMSE(↓)	R(↑), MB(↓), RMSE(↑)	R(↑), MB(↓), RMSE(↓)
	Spring	R(↓), MB(↑), RMSE(↓)	R(↑), MB(↓), RMSE(↑)	R(↓), MB(↑), RMSE(↓)	R(↓), MB(↓), RMSE(↑)	R(↑), MB(↓), RMSE(↓)	R(↓), MB(↓), RMSE(↑)	R(↑), MB(↓), RMSE(↑)
	Summer	R(↑), MB(↑), RMSE(↓)	R(↑), MB(↓), RMSE(↓)	R(↓), MB(↑), RMSE(↓)	R(↑), MB(↓), RMSE(↓)	R(↓), MB(↓), RMSE(↓)	R(↑), MB(↓), RMSE(↓)	R(↑), MB(↓), RMSE(↓)
	Autumn	R(↓), MB(↑), RMSE(↓)	R(↑), MB(↓), RMSE(↑)	R(↓), MB(↑), RMSE(↓)	R(↓), MB(↓), RMSE(↑)	R(↑), MB(↓), RMSE(↓)	R(↓), MB(↓), RMSE(↑)	R(↑), MB(↓), RMSE(↓)
	Winter	R(↑), MB(↑), RMSE(↓)	R(↑), MB(↓), RMSE(↑)	R(↓), MB(↑), RMSE(↑)	R(↑), MB(↓), RMSE(↑)	R(↑), MB(↓), RMSE(↑)	R(↓), MB(↑), RMSE(↑)	R(↓), MB(↓), RMSE(↑)
Precipitation	Annual	R(↑), MB(↓), RMSE(↓)	R(↑), MB(↓), RMSE(↓)	R(↓), MB(↑), RMSE(↑)	R(↓), MB(↑), RMSE(↑)	R(↓), MB(↓), RMSE(↓)	R(↓), MB(↓), RMSE(↑)	R(↓), MB(↓), RMSE(↑)
	Spring	R(↓), MB(↓), RMSE(↓)	R(↓), MB(↓), RMSE(↓)	R(↓), MB(↑), RMSE(↑)	R(↓), MB(↑), RMSE(↑)	R(↑), MB(↓), RMSE(↓)	R(↓), MB(↑), RMSE(↑)	R(↓), MB(↓), RMSE(↑)
	Summer	R(↑), MB(↓), RMSE(↓)	R(↑), MB(↓), RMSE(↓)	R(↓), MB(↑), RMSE(↓)	R(↑), MB(↓), RMSE(↓)	R(↓), MB(↓), RMSE(↓)	R(↑), MB(↓), RMSE(↑)	R(↓), MB(↓), RMSE(↑)
	Autumn	R(↑), MB(↓), RMSE(↓)	R(↓), MB(↓), RMSE(↓)	R(↓), MB(↑), RMSE(↑)	R(↓), MB(↑), RMSE(↑)	R(↓), MB(↓), RMSE(↑)	R(↓), MB(↑), RMSE(↑)	R(↓), MB(↑), RMSE(↑)
	Winter	R(↑), MB(↓), RMSE(↓)	R(↑), MB(↓), RMSE(↓)	R(↓), MB(↑), RMSE(↑)	R(↓), MB(↑), RMSE(↑)	R(↓), MB(↓), RMSE(↓)	R(↓), MB(↓), RMSE(↑)	R(↓), MB(↓), RMSE(↓)
$PM_{2.5}$	Annual	R(↑), MB(↑), RMSE(↑)	R(↑), MB(↑), RMSE(↑)	R(↑), MB(↓), RMSE(↓)	R(↑), MB(↓), RMSE(↓)	R(↑), MB(↑), RMSE(↑)	R(↓), MB(↓), RMSE(↓)	R(↑), MB(↑), RMSE(↑)
	Spring	R(↑), MB(↑), RMSE(↑)	R(↑), MB(↑), RMSE(↑)	R(↑), MB(↓), RMSE(↓)	R(↑), MB(↓), RMSE(↑)	R(↑), MB(↑), RMSE(↑)	R(↓), MB(↑), RMSE(↑)	R(↑), MB(↑), RMSE(↑)
	Summer	R(↑), MB(↑), RMSE(↑)	R(↑), MB(↑), RMSE(↑)	R(↑), MB(↓), RMSE(↑)	R(↑), MB(↓), RMSE(↑)	R(↑), MB(↑), RMSE(↑)	R(↑), MB(↑), RMSE(↑)	R(↑), MB(↑), RMSE(↑)
	Autumn	R(↑), MB(↑), RMSE(↑)	R(↑), MB(↑), RMSE(↑)	R(↑), MB(↓), RMSE(↓)	R(↑), MB(↓), RMSE(↓)	R(↑), MB(↑), RMSE(↑)	R(↑), MB(↓), RMSE(↓)	R(↑), MB(↑), RMSE(↑)
	Winter	R(↑), MB(↑), RMSE(↓)	R(↑), MB(↑), RMSE(↑)	R(↑), MB(↓), RMSE(↓)	R(↑), MB(↓), RMSE(↓)	R(↑), MB(↑), RMSE(↑)	R(↓), MB(↓), RMSE(↓)	R(↑), MB(↑), RMSE(↑)
O_3	Annual	R(↑), MB(↓), RMSE(↑)	R(↓), MB(↓), RMSE(↓)	R(↓), MB(↑), RMSE(↓)	R(↓), MB(↓), RMSE(↓)	R(↓), MB(↓), RMSE(↓)	R(↓), MB(↑), RMSE(↑)	R(↓), MB(↓), RMSE(↑)
	Spring	R(↑), MB(↓), RMSE(↑)	R(↓), MB(↓), RMSE(↑)	R(↓), MB(↓), RMSE(↓)	R(↓), MB(↓), RMSE(↑)	R(↓), MB(↓), RMSE(↓)	R(↓), MB(↑), RMSE(↑)	R(↓), MB(↓), RMSE(↑)
	Summer	R(↓), MB(↑), RMSE(↑)	R(↓), MB(↓), RMSE(↓)	R(↑), MB(↓), RMSE(↓)	R(↓), MB(↓), RMSE(↓)	R(↓), MB(↓), RMSE(↓)	R(↓), MB(↑), RMSE(↑)	R(↓), MB(↓), RMSE(↑)
	Autumn	R(↑), MB(↓), RMSE(↑)	R(↓), MB(↓), RMSE(↓)	R(↓), MB(↑), RMSE(↑)	R(↓), MB(↓), RMSE(↑)	R(↑), MB(↓), RMSE(↓)	R(↓), MB(↑), RMSE(↑)	R(↓), MB(↑), RMSE(↑)
	Winter	R(↓), MB(↓), RMSE(↑)	R(↓), MB(↓), RMSE(↑)	R(↓), MB(↑), RMSE(↓)	R(↓), MB(↓), RMSE(↑)	R(↓), MB(↓), RMSE(↑)	R(↓), MB(↓), RMSE(↓)	R(↓), MB(↓), RMSE(↓)
NO_2	Annual	R(↑), MB(↑), RMSE(↑)	R(↑), MB(↑), RMSE(↓)	R(↑), MB(↓), RMSE(↑)	R(↑), MB(↑), RMSE(↓)	R(↑), MB(↑), RMSE(↓)	R(↓), MB(↑), RMSE(↑)	R(↑), MB(↑), RMSE(↓)
	Spring	R(↑), MB(↑), RMSE(↑)	R(↑), MB(↑), RMSE(↑)	R(↓), MB(↓), RMSE(↑)	R(↑), MB(↑), RMSE(↑)	R(↑), MB(↑), RMSE(↓)	R(↓), MB(↑), RMSE(↑)	R(↑), MB(↑), RMSE(↓)
	Summer	R(↓), MB(↑), RMSE(↑)	R(↑), MB(↑), RMSE(↑)	R(↓), MB(↓), RMSE(↓)	R(↑), MB(↑), RMSE(↑)	R(↓), MB(↑), RMSE(↑)	R(↑), MB(↑), RMSE(↓)	R(↓), MB(↑), RMSE(↑)

	Autumn	R(↑), MB(↑), RMSE(↑)	R(↑), MB(↑), RMSE(↓)	R(↑), MB(↓), RMSE(↑)	R(↑), MB(↑), RMSE(↓)	R(↓), MB(↑), RMSE(↑)	R(↑), MB(↓), RMSE(↑)	R(↓), MB(↑), RMSE(↑)
	Winter	R(↑), MB(↑), RMSE(↑)	R(↑), MB(↑), RMSE(↓)	R(↑), MB(↓), RMSE(↑)	R(↑), MB(↑), RMSE(↓)	R(↑), MB(↑), RMSE(↓)	R(↓), MB(↑), RMSE(↑)	R(↓), MB(↑), RMSE(↓)
SO_2	Annual	R(↑), MB(↑), RMSE(↑)	R(↓), MB(↑), RMSE(↓)	R(↑), MB(↓), RMSE(↑)	R(↑), MB(↓), RMSE(↑)	R(↑), MB(↑), RMSE(↑)	R(↓), MB(↑), RMSE(↑)	R(↑), MB(↑), RMSE(↑)
	Spring	R(↑), MB(↑), RMSE(↑)	R(↓), MB(↑), RMSE(↓)	R(↑), MB(↓), RMSE(↑)	R(↑), MB(↓), RMSE(↑)	R(↑), MB(↑), RMSE(↑)	R(↓), MB(↑), RMSE(↑)	R(↓), MB(↑), RMSE(↑)
	Summer	R(↑), MB(↑), RMSE(↑)	R(↑), MB(↑), RMSE(↑)	R(↑), MB(↓), RMSE(↑)	R(↑), MB(↓), RMSE(↑)	R(↑), MB(↑), RMSE(↓)	R(↓), MB(↑), RMSE(↓)	R(↑), MB(↑), RMSE(↓)
	Autumn	R(↑), MB(↑), RMSE(↑)	R(↓), MB(↑), RMSE(↓)	R(↑), MB(↓), RMSE(↑)	R(↑), MB(↓), RMSE(↑)	R(↓), MB(↑), RMSE(↑)	R(↑), MB(↓), RMSE(↓)	R(↓), MB(↑), RMSE(↑)
	Winter	R(↑), MB(↑), RMSE(↑)	R(↓), MB(↑), RMSE(↓)	R(↑), MB(↓), RMSE(↑)	R(↑), MB(↓), RMSE(↑)	R(↑), MB(↑), RMSE(↑)	R(↓), MB(↑), RMSE(↑)	R(↑), MB(↑), RMSE(↑)
CO	Annual	R(↑), MB(↑), RMSE(↑)	R(↑), MB(↑), RMSE(↑)	R(↓), MB(↓), RMSE(↑)	R(↑), MB(↑), RMSE(↑)	R(↑), MB(↑), RMSE(↑)	R(↓), MB(↓), RMSE(↑)	R(↑), MB(↑), RMSE(↑)
	Spring	R(↑), MB(↑), RMSE(↑)	R(↑), MB(↑), RMSE(↑)	R(↓), MB(↓), RMSE(↑)	R(↓), MB(↑), RMSE(↑)	R(↑), MB(↑), RMSE(↑)	R(↓), MB(↓), RMSE(↑)	R(↑), MB(↑), RMSE(↑)
	Summer	R(↑), MB(↑), RMSE(↑)	R(↑), MB(↑), RMSE(↑)	R(↓), MB(↓), RMSE(↑)	R(↓), MB(↓), RMSE(↑)	R(↓), MB(↓), RMSE(↑)	R(↓), MB(↓), RMSE(↑)	R(↓), MB(↓), RMSE(↑)
	Autumn	R(↑), MB(↑), RMSE(↑)	R(↑), MB(↑), RMSE(↑)	R(↓), MB(↓), RMSE(↑)	R(↑), MB(↑), RMSE(↑)	R(↑), MB(↑), RMSE(↑)	R(↑), MB(↓), RMSE(↑)	R(↑), MB(↑), RMSE(↑)
	Winter	R(↑), MB(↑), RMSE(↓)	R(↑), MB(↑), RMSE(↓)	R(↑), MB(↓), RMSE(↑)	R(↑), MB(↑), RMSE(↓)	R(↑), MB(↑), RMSE(↓)	R(↓), MB(↓), RMSE(↑)	R(↑), MB(↑), RMSE(↓)

Satellite observations		WRF-CMAQ_ARI	WRF-Chem_ARI	WRF-Chem_ACI	WRF-Chem_BOTH	WRF-CHIMERE_ARI	WRF-CHIMERE_ACI	WRF-CHIMERE_BOTH
SSR	Annual	R(↓), MB(↓), RMSE(↓)	R(↑), MB(↓), RMSE(↓)	R(↓), MB(↑), RMSE(↑)	R(↑), MB(↓), RMSE(↓)	R(↑), MB(↓), RMSE(↓)	R(↑), MB(↑), RMSE(↑)	R(↑), MB(↓), RMSE(↓)
	Spring	R(↑), MB(↓), RMSE(↓)	R(↑), MB(↓), RMSE(↓)	R(↑), MB(↑), RMSE(↑)	R(↑), MB(↓), RMSE(↓)	R(↑), MB(↓), RMSE(↓)	R(↓), MB(↓), RMSE(↑)	R(↑), MB(↓), RMSE(↓)
	Summer	R(↑), MB(↓), RMSE(↓)	R(↑), MB(↓), RMSE(↓)	R(↓), MB(↑), RMSE(↑)	R(↑), MB(↓), RMSE(↓)	R(↑), MB(↓), RMSE(↓)	R(↓), MB(↑), RMSE(↑)	R(↑), MB(↓), RMSE(↓)
	Autumn	R(↓), MB(↓), RMSE(↓)	R(↑), MB(↓), RMSE(↓)	R(↓), MB(↑), RMSE(↑)	R(↑), MB(↓), RMSE(↓)	R(↑), MB(↓), RMSE(↓)	R(↓), MB(↑), RMSE(↑)	R(↓), MB(↓), RMSE(↓)
	Winter	R(↓), MB(↓), RMSE(↓)	R(↑), MB(↓), RMSE(↓)	R(↑), MB(↑), RMSE(↓)	R(↑), MB(↑), RMSE(↓)	R(↑), MB(↓), RMSE(↓)	R(↓), MB(↓), RMSE(↑)	R(↓), MB(↓), RMSE(↓)
SLR	Annual	R(↓), MB(↓), RMSE(↑)	R(↑), MB(↓), RMSE(↑)	R(↓), MB(↓), RMSE(↑)	R(↑), MB(↓), RMSE(↑)	R(↓), MB(↑), RMSE(↓)	R(↓), MB(↓), RMSE(↑)	R(↓), MB(↑), RMSE(↓)
	Spring	R(↓), MB(↓), RMSE(↑)	R(↑), MB(↓), RMSE(↑)	R(↓), MB(↓), RMSE(↑)	R(↑), MB(↓), RMSE(↑)	R(↓), MB(↑), RMSE(↓)	R(↑), MB(↓), RMSE(↑)	R(↓), MB(↑), RMSE(↓)
	Summer	R(↓), MB(↓), RMSE(↑)	R(↑), MB(↓), RMSE(↑)	R(↓), MB(↓), RMSE(↑)	R(↑), MB(↓), RMSE(↑)	R(↑), MB(↑), RMSE(↓)	R(↓), MB(↑), RMSE(↑)	R(↑), MB(↑), RMSE(↓)
	Autumn	R(↑), MB(↓), RMSE(↑)	R(↑), MB(↓), RMSE(↑)	R(↓), MB(↓), RMSE(↑)	R(↑), MB(↓), RMSE(↑)	R(↓), MB(↑), RMSE(↓)	R(↓), MB(↓), RMSE(↑)	R(↓), MB(↑), RMSE(↓)
	Winter	R(↓), MB(↓), RMSE(↑)	R(↓), MB(↓), RMSE(↑)	R(↓), MB(↓), RMSE(↑)	R(↓), MB(↓), RMSE(↑)	R(↑), MB(↑), RMSE(↓)	R(↓), MB(↓), RMSE(↑)	R(↑), MB(↑), RMSE(↓)
TSR	Annual	R(↓), MB(↑), RMSE(↑)	R(↓), MB(↑), RMSE(↓)	R(↓), MB(↓), RMSE(↑)	R(↓), MB(↓), RMSE(↑)	R(↑), MB(↑), RMSE(↓)	R(↑), MB(↓), RMSE(↓)	R(↑), MB(↓), RMSE(↓)
	Spring	R(↓), MB(↑), RMSE(↓)	R(↓), MB(↓), RMSE(↓)	R(↓), MB(↓), RMSE(↑)	R(↓), MB(↓), RMSE(↓)	R(↑), MB(↑), RMSE(↓)	R(↓), MB(↓), RMSE(↓)	R(↓), MB(↓), RMSE(↓)
	Summer	R(↓), MB(↑), RMSE(↑)	R(↓), MB(↓), RMSE(↓)	R(↓), MB(↓), RMSE(↑)	R(↓), MB(↓), RMSE(↓)	R(↑), MB(↑), RMSE(↓)	R(↑), MB(↓), RMSE(↓)	R(↑), MB(↓), RMSE(↓)
	Autumn	R(↓), MB(↑), RMSE(↑)	R(↓), MB(↑), RMSE(↓)	R(↓), MB(↓), RMSE(↑)	R(↓), MB(↓), RMSE(↑)	R(↑), MB(↑), RMSE(↓)	R(↓), MB(↓), RMSE(↓)	R(↓), MB(↓), RMSE(↓)
	Winter	R(↑), MB(↑), RMSE(↓)	R(↑), MB(↑), RMSE(↓)	R(↓), MB(↓), RMSE(↓)	R(↓), MB(↓), RMSE(↓)	R(↑), MB(↑), RMSE(↓)	R(↑), MB(↓), RMSE(↓)	R(↑), MB(↑), RMSE(↓)

TLR	Annual	R(↑), MB(↑), RMSE(↓)	R(↑), MB(↓), RMSE(↓)	R(↑), MB(↑), RMSE(↓)	R(↑), MB(↑), RMSE(↓)	R(↑), MB(↓), RMSE(↓)	R(↑), MB(↑), RMSE(↓)	R(↑), MB(↑), RMSE(↓)
	Spring	R(↑), MB(↑), RMSE(↓)	R(↑), MB(↓), RMSE(↑)	R(↑), MB(↑), RMSE(↓)	R(↑), MB(↓), RMSE(↓)	R(↓), MB(↓), RMSE(↓)	R(↑), MB(↑), RMSE(↓)	R(↑), MB(↑), RMSE(↓)
	Summer	R(↑), MB(↑), RMSE(↓)	R(↓), MB(↓), RMSE(↓)	R(↑), MB(↑), RMSE(↓)	R(↑), MB(↓), RMSE(↓)	R(↑), MB(↓), RMSE(↓)	R(↓), MB(↑), RMSE(↓)	R(↓), MB(↑), RMSE(↓)
	Autumn	R(↑), MB(↑), RMSE(↓)	R(↑), MB(↓), RMSE(↓)	R(↑), MB(↑), RMSE(↑)	R(↑), MB(↓), RMSE(↓)	R(↑), MB(↓), RMSE(↓)	R(↑), MB(↑), RMSE(↓)	R(↑), MB(↑), RMSE(↓)
	Winter	R(↑), MB(↓), RMSE(↓)	R(↑), MB(↓), RMSE(↓)	R(↑), MB(↑), RMSE(↑)	R(↑), MB(↑), RMSE(↑)	R(↑), MB(↓), RMSE(↑)	R(↑), MB(↑), RMSE(↓)	R(↑), MB(↑), RMSE(↓)
Precipitation	Annual	R(↓), MB(↑), RMSE(↑)	R(↑), MB(↓), RMSE(↓)	R(↓), MB(↑), RMSE(↑)	R(↓), MB(↑), RMSE(↑)	R(↓), MB(↓), RMSE(↑)	R(↑), MB(↑), RMSE(↑)	R(↓), MB(↓), RMSE(↑)
	Spring	R(↓), MB(↓), RMSE(↑)	R(↓), MB(↓), RMSE(↓)	R(↓), MB(↑), RMSE(↑)	R(↓), MB(↑), RMSE(↑)	R(↑), MB(↑), RMSE(↓)	R(↑), MB(↓), RMSE(↓)	R(↑), MB(↓), RMSE(↓)
	Summer	R(↓), MB(↓), RMSE(↑)	R(↑), MB(↓), RMSE(↓)	R(↓), MB(↑), RMSE(↑)	R(↓), MB(↑), RMSE(↑)	R(↓), MB(↓), RMSE(↑)	R(↓), MB(↑), RMSE(↑)	R(↓), MB(↑), RMSE(↑)
	Autumn	R(↓), MB(↓), RMSE(↑)	R(↑), MB(↓), RMSE(↓)	R(↓), MB(↑), RMSE(↑)	R(↓), MB(↑), RMSE(↑)	R(↑), MB(↓), RMSE(↑)	R(↓), MB(↑), RMSE(↑)	R(↓), MB(↑), RMSE(↑)
	Winter	R(↑), MB(↑), RMSE(↑)	R(↑), MB(↓), RMSE(↓)	R(↑), MB(↑), RMSE(↑)	R(↑), MB(↑), RMSE(↑)	R(↑), MB(↓), RMSE(↓)	R(↑), MB(↓), RMSE(↓)	R(↑), MB(↓), RMSE(↓)
CF	Annual	R(↓), MB(↑), RMSE(↓)	R(↓), MB(↓), RMSE(↑)	R(↓), MB(↓), RMSE(↑)	R(↓), MB(↓), RMSE(↑)	R(↓), MB(↓), RMSE(↑)	R(↓), MB(↑), RMSE(↑)	R(↓), MB(↑), RMSE(↑)
	Spring	R(↓), MB(↑), RMSE(↓)	R(↓), MB(↓), RMSE(↓)	R(↓), MB(↓), RMSE(↓)	R(↓), MB(↓), RMSE(↓)	R(↓), MB(↓), RMSE(↓)	R(↓), MB(↑), RMSE(↑)	R(↓), MB(↑), RMSE(↑)
	Summer	R(↓), MB(↑), RMSE(↑)	R(↓), MB(↓), RMSE(↓)	R(↓), MB(↓), RMSE(↓)	R(↓), MB(↓), RMSE(↓)	R(↓), MB(↓), RMSE(↓)	R(↓), MB(↑), RMSE(↑)	R(↓), MB(↑), RMSE(↑)
	Autumn	R(↓), MB(↑), RMSE(↓)	R(↓), MB(↓), RMSE(↓)	R(↓), MB(↓), RMSE(↓)	R(↓), MB(↓), RMSE(↓)	R(↑), MB(↓), RMSE(↓)	R(↓), MB(↑), RMSE(↑)	R(↓), MB(↑), RMSE(↑)
	Winter	R(↑), MB(↑), RMSE(↓)	R(↓), MB(↓), RMSE(↓)	R(↓), MB(↓), RMSE(↓)	R(↓), MB(↓), RMSE(↓)	R(↓), MB(↓), RMSE(↓)	R(↓), MB(↑), RMSE(↑)	R(↓), MB(↑), RMSE(↑)
LWP	Annual	R(↓), MB(↑), RMSE(↓)	R(↓), MB(↓), RMSE(↑)	R(↓), MB(↓), RMSE(↑)	R(↓), MB(↓), RMSE(↑)	R(↓), MB(↓), RMSE(↑)	R(↓), MB(↓), RMSE(↑)	R(↓), MB(↓), RMSE(↑)
	Spring	R(↓), MB(↑), RMSE(↓)	R(↓), MB(↓), RMSE(↑)	R(↓), MB(↓), RMSE(↑)	R(↓), MB(↓), RMSE(↑)	R(↓), MB(↑), RMSE(↑)	R(↓), MB(↓), RMSE(↑)	R(↓), MB(↓), RMSE(↑)
	Summer	R(↓), MB(↑), RMSE(↓)	R(↓), MB(↓), RMSE(↑)	R(↓), MB(↓), RMSE(↑)	R(↓), MB(↓), RMSE(↑)	R(↓), MB(↓), RMSE(↑)	R(↓), MB(↓), RMSE(↑)	R(↓), MB(↓), RMSE(↑)
	Autumn	R(↓), MB(↑), RMSE(↑)	R(↓), MB(↓), RMSE(↑)	R(↓), MB(↓), RMSE(↑)	R(↓), MB(↓), RMSE(↑)	R(↑), MB(↑), RMSE(↓)	R(↓), MB(↓), RMSE(↓)	R(↓), MB(↓), RMSE(↓)
	Winter	R(↓), MB(↑), RMSE(↑)	R(↓), MB(↓), RMSE(↑)	R(↓), MB(↑), RMSE(↑)	R(↓), MB(↑), RMSE(↑)	R(↑), MB(↓), RMSE(↑)	R(↑), MB(↑), RMSE(↑)	R(↑), MB(↑), RMSE(↑)
AOD	Annual	R(↓), MB(↑), RMSE(↑)	R(↓), MB(↑), RMSE(↑)	R(↓), MB(↓), RMSE(↓)	R(↓), MB(↓), RMSE(↓)	R(↓), MB(↑), RMSE(↑)	R(↓), MB(↑), RMSE(↑)	R(↓), MB(↑), RMSE(↑)
	Spring	R(↓), MB(↑), RMSE(↑)	R(↓), MB(↑), RMSE(↑)	R(↓), MB(↓), RMSE(↓)	R(↓), MB(↓), RMSE(↓)	R(↓), MB(↑), RMSE(↓)	R(↓), MB(↑), RMSE(↓)	R(↓), MB(↑), RMSE(↓)
	Summer	R(↑), MB(↑), RMSE(↓)	R(↑), MB(↑), RMSE(↑)	R(↓), MB(↓), RMSE(↑)	R(↓), MB(↓), RMSE(↑)	R(↓), MB(↑), RMSE(↑)	R(↑), MB(↑), RMSE(↓)	R(↓), MB(↑), RMSE(↓)
	Autumn	R(↑), MB(↑), RMSE(↓)	R(↑), MB(↑), RMSE(↑)	R(↓), MB(↓), RMSE(↓)	R(↓), MB(↓), RMSE(↓)	R(↑), MB(↑), RMSE(↑)	R(↓), MB(↑), RMSE(↑)	R(↓), MB(↑), RMSE(↑)
	Winter	R(↓), MB(↑), RMSE(↑)	R(↓), MB(↑), RMSE(↑)	R(↓), MB(↓), RMSE(↓)	R(↓), MB(↓), RMSE(↓)	R(↓), MB(↑), RMSE(↑)	R(↓), MB(↑), RMSE(↑)	R(↓), MB(↑), RMSE(↑)
O3 VCDs	Annual	R(↑), MB(↑), RMSE(↑)	R(↓), MB(↓), RMSE(↑)	R(↓), MB(↓), RMSE(↑)	R(↓), MB(↓), RMSE(↑)	R(↑), MB(↓), RMSE(↓)	R(↓), MB(↑), RMSE(↑)	R(↓), MB(↑), RMSE(↓)
	Spring	R(↑), MB(↑), RMSE(↑)	R(↑), MB(↑), RMSE(↑)	R(↓), MB(↓), RMSE(↑)	R(↓), MB(↓), RMSE(↑)	R(↓), MB(↓), RMSE(↓)	R(↑), MB(↑), RMSE(↓)	R(↑), MB(↓), RMSE(↓)
	Summer	R(↑), MB(↑), RMSE(↑)	R(↓), MB(↓), RMSE(↑)	R(↓), MB(↓), RMSE(↑)	R(↓), MB(↓), RMSE(↑)	R(↑), MB(↓), RMSE(↓)	R(↓), MB(↑), RMSE(↑)	R(↑), MB(↑), RMSE(↓)

	Autumn	R(↑), MB(↑), RMSE(↑)	R(↑), MB(↓), RMSE(↑)	R(↓), MB(↓), RMSE(↑)	R(↓), MB(↓), RMSE(↑)	R(↓), MB(↓), RMSE(↑)	R(↓), MB(↑), RMSE(↑)	R(↓), MB(↑), RMSE(↑)
	Winter	R(↑), MB(↑), RMSE(↑)	R(↓), MB(↑), RMSE(↓)	R(↓), MB(↓), RMSE(↑)	R(↓), MB(↓), RMSE(↑)	R(↓), MB(↑), RMSE(↓)	R(↑), MB(↓), RMSE(↓)	R(↑), MB(↓), RMSE(↓)
NO_2 VCDs	Annual	R(↑), MB(↑), RMSE(↑)	R(↑), MB(↑), RMSE(↑)	R(↓), MB(↓), RMSE(↓)	R(↑), MB(↓), RMSE(↓)	R(↓), MB(↑), RMSE(↑)	R(↓), MB(↓), RMSE(↑)	R(↓), MB(↑), RMSE(↑)
	Spring	R(↑), MB(↑), RMSE(↑)	R(↑), MB(↑), RMSE(↓)	R(↓), MB(↓), RMSE(↑)	R(↑), MB(↓), RMSE(↓)	R(↓), MB(↑), RMSE(↓)	R(↑), MB(↓), RMSE(↓)	R(↓), MB(↑), RMSE(↓)
	Summer	R(↓), MB(↑), RMSE(↑)	R(↑), MB(↑), RMSE(↑)	R(↓), MB(↓), RMSE(↓)	R(↓), MB(↓), RMSE(↑)	R(↑), MB(↑), RMSE(↑)	R(↓), MB(↓), RMSE(↑)	R(↓), MB(↑), RMSE(↑)
	Autumn	R(↑), MB(↑), RMSE(↑)	R(↑), MB(↑), RMSE(↓)	R(↓), MB(↓), RMSE(↑)	R(↓), MB(↓), RMSE(↑)	R(↓), MB(↑), RMSE(↓)	R(↑), MB(↓), RMSE(↑)	R(↑), MB(↓), RMSE(↓)
	Winter	R(↓), MB(↑), RMSE(↑)	R(↑), MB(↑), RMSE(↓)	R(↑), MB(↓), RMSE(↓)	R(↑), MB(↓), RMSE(↓)	R(↓), MB(↑), RMSE(↓)	R(↑), MB(↑), RMSE(↓)	R(↑), MB(↑), RMSE(↓)
SO_2 VCDs	Annual	R(↓), MB(↑), RMSE(↓)	R(↓), MB(↑), RMSE(↓)	R(↓), MB(↓), RMSE(↓)	R(↓), MB(↓), RMSE(↓)	R(↑), MB(↑), RMSE(↑)	R(↓), MB(↓), RMSE(↑)	R(↓), MB(↑), RMSE(↓)
	Spring	R(↑), MB(↑), RMSE(↑)	R(↓), MB(↑), RMSE(↑)	R(↓), MB(↓), RMSE(↓)	R(↓), MB(↓), RMSE(↓)	R(↑), MB(↑), RMSE(↑)	R(↓), MB(↓), RMSE(↑)	R(↓), MB(↑), RMSE(↑)
	Summer	R(↑), MB(↑), RMSE(↑)	R(↓), MB(↑), RMSE(↑)	R(↓), MB(↓), RMSE(↓)	R(↓), MB(↓), RMSE(↓)	R(↓), MB(↑), RMSE(↑)	R(↓), MB(↑), RMSE(↑)	R(↓), MB(↑), RMSE(↑)
	Autumn	R(↓), MB(↑), RMSE(↑)	R(↑), MB(↑), RMSE(↑)	R(↓), MB(↓), RMSE(↑)	R(↓), MB(↓), RMSE(↑)	R(↑), MB(↑), RMSE(↑)	R(↑), MB(↓), RMSE(↓)	R(↑), MB(↑), RMSE(↑)
	Winter	R(↓), MB(↑), RMSE(↑)	R(↓), MB(↑), RMSE(↑)	R(↑), MB(↓), RMSE(↓)	R(↓), MB(↓), RMSE(↓)	R(↓), MB(↑), RMSE(↑)	R(↓), MB(↓), RMSE(↓)	R(↓), MB(↑), RMSE(↑)
CO VCDs	Annual	R(↓), MB(↑), RMSE(↓)	R(↑), MB(↑), RMSE(↓)	R(↑), MB(↑), RMSE(↑)	R(↑), MB(↑), RMSE(↑)	R(↓), MB(↑), RMSE(↑)	R(↓), MB(↓), RMSE(↑)	R(↓), MB(↑), RMSE(↑)
	Spring	R(↓), MB(↑), RMSE(↓)	R(↑), MB(↑), RMSE(↓)	R(↑), MB(↑), RMSE(↓)	R(↑), MB(↑), RMSE(↓)	R(↓), MB(↑), RMSE(↓)	R(↓), MB(↓), RMSE(↑)	R(↓), MB(↑), RMSE(↑)
	Summer	R(↓), MB(↑), RMSE(↑)	R(↑), MB(↑), RMSE(↓)	R(↑), MB(↑), RMSE(↑)	R(↑), MB(↑), RMSE(↑)	R(↓), MB(↓), RMSE(↑)	R(↑), MB(↓), RMSE(↓)	R(↑), MB(↓), RMSE(↑)
	Autumn	R(↓), MB(↑), RMSE(↑)	R(↑), MB(↑), RMSE(↑)	R(↑), MB(↑), RMSE(↑)	R(↑), MB(↑), RMSE(↑)	R(↓), MB(↑), RMSE(↑)	R(↑), MB(↓), RMSE(↓)	R(↑), MB(↑), RMSE(↑)
	Winter	R(↓), MB(↑), RMSE(↑)	R(↓), MB(↓), RMSE(↑)	R(↑), MB(↑), RMSE(↓)	R(↓), MB(↑), RMSE(↓)	R(↓), MB(↑), RMSE(↑)	R(↓), MB(↓), RMSE(↑)	R(↓), MB(↑), RMSE(↑)
NH_3 VCDs	Annual	R(↓), MB(↑), RMSE(↑)	R(↓), MB(↓), RMSE(↓)	R(↑), MB(↓), RMSE(↑)	R(↑), MB(↓), RMSE(↑)	N/A	N/A	N/A
	Spring	R(↓), MB(↑), RMSE(↑)	R(↓), MB(↑), RMSE(↑)	R(↓), MB(↓), RMSE(↑)	R(↓), MB(↓), RMSE(↑)	N/A	N/A	N/A
	Summer	R(↓), MB(↑), RMSE(↑)	R(↓), MB(↓), RMSE(↓)	R(↑), MB(↓), RMSE(↓)	R(↑), MB(↓), RMSE(↓)	N/A	N/A	N/A
	Autumn	R(↓), MB(↑), RMSE(↑)	R(↓), MB(↓), RMSE(↑)	R(↑), MB(↓), RMSE(↑)	R(↑), MB(↓), RMSE(↑)	N/A	N/A	N/A
	Winter	R(↑), MB(↑), RMSE(↑)	R(↑), MB(↑), RMSE(↑)	R(↑), MB(↓), RMSE(↑)	R(↑), MB(↓), RMSE(↑)	N/A	N/A	N/A

Table S5. Radiation variables used in the two-way coupled WRF-CMAQ, WRF-Chem and WRF-CHIMERE models with only enabling ARI compared to without aerosol feedbacks.

Model	SW/LW radiation schemes	Turning off feedback	Turning on ARI feedback	
			Direct effects	Semi-direct effects
WRF-CMAQ	RRTMG/RRTMG	Aerosol optical properties are not calculated	Aerosol extinction, single scattering albedo (ω_o), and asymmetry factor (g) 14 shortwave bands and 5 longwave bands (Wong et al., 2012)	1. Solar uv and ir fluxes 2. Radiative heating rate for the tten1d variable
WRF-Chem	RRTMG/RRTMG	Aerosol optical properties are not calculated	ω_o (300 nm, 400 nm, 600 nm, 999 nm), g (300 nm, 400 nm, 600 nm, 999 nm), AOD (τ) (300 nm, 400 nm, 600 nm, 999 nm, 16 bands 3400 nm to 55600 nm) (Zhao et al., 2011)	1. Solar uv and ir fluxes 2. Radiative heating rate for the tten1d variable
WRF-CHIMERE	RRTMG/RRTMG	Aerosol optical properties are not calculated	ω_o (400 nm, 600 nm), g (400 nm, 600 nm), AOD (300 nm, 400 nm, 999 nm, 16 bands 3400 nm to 55600 nm) (Briant et al., 2017)	1. Solar uv and ir fluxes 2. Radiative heating rate for the tten1d variable

Table S6. Description of refractive indices and radiation schemes used in the WRF-CMAQ, WRF-Chem and WRF-CHIMERE models.

Model	Refractive indices of aerosol species groups	
	SW	LW
WRF-CMAQ	1. Water (1.408+1.420×10^{-2}i, 1.324+1.577×10^{-1}i, 1.277+1.516×10^{-3}i, 1.302+1.159×10^{-3}i, 1.312+2.360×10^{-4}i, 1.321+1.713×10^{-4}i, 1.323+2.425×10^{-5}i, 1.327+3.125×10^{-6}i, 1.331+3.405×10^{-8}i, 1.334+1.639×10^{-9}i, 1.340+2.955×10^{-9}i, 1.349+1.635×10^{-8}i, 1.362+3.350×10^{-8}i, 1.260+6.220×10^{-2}i) 2. Water-soluble (1.443+5.718×10^{-3}i, 1.420+1.777×10^{-2}i, 1.420+1.060×10^{-2}i, 1.420+8.368×10^{-3}i, 1.463+1.621×10^{-2}i, 1.510+2.198×10^{-2}i, 1.510+1.929×10^{-2}i, 1.520+1.564×10^{-2}i, 1.530+7.000×10^{-3}i, 1.530+5.666×10^{-3}i, 1.530+5.000×10^{-3}i, 1.530+8.440×10^{-3}i, 1.530+3.000×10^{-2}i, 1.710+1.100×10^{-1}i) 3. BC (2.089+1.070i, 2.014+0.939i, 1.962+0.843i, 1.950+0.784i, 1.940+0.760i, 1.930+0.749i, 1.905+0.737i, 1.870+0.726i, 1.850+0.710i, 1.850+0.710i, 1.850+0.710i, 1.850+0.710i, 1.850+0.710i, 2.589+1.771i) 4. Insoluble (1.272+1.165×10^{-2}i, 1.168+1.073×10^{-2}i, 1.208+8.650×10^{-3}i, 1.253+8.092×10^{-3}i, 1.329+8.000×10^{-3}i, 1.418+8.000×10^{-3}i, 1.456+8.000×10^{-3}i, 1.518+8.000×10^{-3}i, 1.530+8.000×10^{-3}i, 1.530+8.000×10^{-3}i, 1.530+8.000×10^{-3}i, 1.530+8.440×10^{-3}i, 1.530+3.000×10^{-2}i, 1.470+9.000×10^{-2}i) 5. Sea-salt (1.480+1.758×10^{-3}i, 1.534+7.462×10^{-3}i, 1.437+2.950×10^{-3}i, 1.448+1.276×10^{-3}i, 1.450+7.944×10^{-4}i, 1.462+5.382×10^{-4}i, 1.469+3.754×10^{-4}i, 1.470+1.498×10^{-4}i, 1.490+2.050×10^{-7}i, 1.500+1.184×10^{-8}i, 1.502+9.938×10^{-8}i, 1.510+2.060×10^{-6}i, 1.510+5.000×10^{-6}i, 1.510+1.000×10^{-2}i) in terms of 14 wavelengths at 3.4615, 2.7885, 2.325, 2.046, 1.784, 1.4625, 1.2705, 1.0101, 0.7016, 0.53325, 0.38815, 0.299, 0.2316, 8.24 μm	1. Water (1.160+0.321i, 1.140+0.117i, 1.232+0.047i, 1.266+0.038i, 1.300+0.034i) 2. Water-soluble (1.570+0.069i, 1.700+0.055i, 1.890+0.128i, 2.233+0.334i, 1.220+0.066i) 3. BC (1.570+2.200i, 1.700+2.200i, 1.890+2.200i, 2.233+2.200i, 1.220+2.200i) 4. Insoluble (1.482+0.096i, 1.600+0.107i, 1.739+0.162i, 1.508+0.117i, 1.175+0.042i) 5. Sea-salt (1.410+0.019i, 1.490+0.014i, 1.560+0.017i, 1.600+0.029i, 1.402+0.012i) in terms of 5 thermal windows at 13.240, 11.20, 9.73, 8.870, 7.830 μm
WRF-Chem	1. Water (1.35+1.524×10^{-8}i, 1.34+2.494×10^{-9}i, 1.33+1.638×10^{-9}i, 1.33+3.128×10^{-6}i) 2. Dust (1.55+0.003i, 1.550+0.003i, 1.550+0.003i, 1.550+0.003i) 3. BC (1.95+0.79i, 1.95+0.79i, 1.95+0.79i, 1.95+0.79i) 4. OC (1.45+0i, 1.45+0i, 1.45+0i, 1.45+0i) 5. Sea salt (1.51+8.66×10^{-7}i, 1.5+7.019×10^{-8}i, 1.5+1.184×10^{-8}i, 1.47+1.5×10^{-4}i) 6. Sulfate (1.52+1.00×10^{-9}i, 1.52+1.00×10^{-9}i, 1.52+1.00×10^{-9}i, 1.52+1.75×10^{-6}i) in terms of 4 spectral intervals in 0.25-0.35, 0.35-0.45, 0.55-0.65, 0.998-1.000 μm	1. Water (1.532+0.336i, 1.524+0.360i, 1.420+0.426i, 1.274+0.403i, 1.161+0.321i, 1.142+0.115i, 1.232+0.0471i, 1.266+0.039i, 1.296+0.034i, 1.321+0.0344i, 1.342+0.092i, 1.315+0.012i, 1.330+0.013i, 1.339+0.01i, 1.350+0.0049i, 1.408+0.0142i) 2. Dust (2.34+0.7i, 2.904+0.857i, 1.748+0.462i, 1.508+0.263i, 1.911+0.319i, 1.822+0.26i, 2.917+0.65i, 1.557+0.373i, 1.242+0.093i, 1.447+0.105i, 1.432+0.061i, 1.473+0.0245i, 1.495+0.011i, 1.5+0.008i) 3. BC (1.95+0.79i, 1.95+0.79i, 1.95+0.79i, 1.95+0.79i, 1.95+0.79i, 1.95+0.79i, 1.95+0.79i, 1.95+0.79i, 1.95+0.79i, 1.95+0.79i, 1.95+0.79i, 1.95+0.79i, 1.95+0.79i, 1.95+0.79i,) 4. OC (1.86+0.5i, 1.91+0.268i, 1.988+0.185i, 1.439+0.198i, 1.606+0.059i, 1.7+0.0488i, 1.888+0.11i, 2.489+0.3345i, 1.219+0.065i, 1.419+0.058i, 1.426+0.0261i, 1.446+0.0142i, 1.457+0.013i, 1.458+0.01i) 5. Sea salt (1.74+0.1978i, 1.76+0.1978i, 1.78+0.129i, 1.456+0.038i, 1.41+0.019i, 1.48+0.014i, 1.56+0.016i, 1.63+0.03i, 1.4+0.012i, 1.43+0.0064i, 1.56+0.0196i, 1.45+0.0029i, 1.485+0.0017i, 1.486+0.0014i) 6. Sulfate (1.89+0.22i, 1.91+0.152i, 1.93+0.0846i, 1.586+0.2225i, 1.678+0.195i, 1.758+0.441i, 1.855+0.696i, 1.597+0.695i, 1.15+0.459i, 1.26+0.161i, 1.42+0.172i, 1.35+0.14i, 1.379+0.12i, 1.385+0.122i) in terms of 16 spectral intervals in 10-350, 350-500, 500-630, 630-700, 700-820, 820-980, 980-1080, 1080-1180, 1180-1390, 1390-1480, 1480-1800, 1800-2080, 2080-2250, 2250-2390, 2390-2600, 2600-3250 cm^{-1}
WRF-CHIMERE	1. Water (1.35+2.0×10^{-9}i, 1.34+2.0×10^{-9}i, 1.34+1.8×10^{-8}i, 1.33+3.4×10^{-8}i, 1.33+3.9×10^{-7}i) 2. Dust (1.53+0.0055i, 1.53+0.0055i, 1.53+0.0024i, 1.53+8.9-4i, 1.53+7.6-4i) 3. BC (1.95+0.79i, 1.95+0.79i, 1.95+0.79i, 1.95+0.79i, 1.95+0.79i) 4. OC (1.53+0.09i, 1.53+0.008i, 1.53+0.005i, 1.53+0.0063i, 1.52+0.016i) 5. Sea salt (1.38+8.7×10^{-7}i, 1.38+3.5×10^{-7}i, 1.37+6.6×10^{-9}i, 1.36+1.2×10^{-8}i, 1.35+2.6×10^{-5}i) 6. PPM (1.53+0.008i, 1.52+0.008i, 1.52+0.008i, 1.51+0.008i, 1.5+0.008i) 7. SOA (1.56+0.003i, 1.56+0.003i, 1.56+0.003i, 1.56+0.003i, 1.56+0.003i) 8. H_2SO_4 (1.5+1.0×10^{-8}i, 1.47+1.0×10^{-8}i, 1.44+1.0×10^{-8}i, 1.43+1.3×10^{-8}i, 1.42+1.2×10^{-6}i) 9. HNO_3 (1.53+0.006i, 1.53+0.006i, 1.53+0.006i, 1.53+0.006i, 1.53+0.006i) 10. NH_3 (1.53+0.0005i, 1.52+0.0005i, 1.52+0.0005i, 1.52+0.0005i, 1.52+0.0005i) in terms of 5 wavelengths at 0.2, 0.3, 0.4, 0.6, 0.999 μm	1. Water (1.42+0.02i, 1.35+0.0047i, 1.34+0.0085i, 1.33+0.015i, 1.32+0.01i, 1.32+0.13i, 1.32+0.032i, 1.3+0.034i, 1.27+0.039i, 1.23+0.047i, 1.15+0.1i, 1.16+0.32i, 1.27+0.4i, 1.41+0.43i, 1.52+0.37i, 1.65+0.55i) 2. BC (1.95+0.79i, 1.95+0.79i, 1.95+0.79i, 1.95+0.79i, 1.95+0.79i, 1.95+0.79i, 1.95+0.79i, 1.95+0.79i, 1.95+0.79i, 1.95+0.79i, 1.95+0.79i, 1.95+0.79i, 1.95+0.79i, 1.95+0.79i, 1.95+0.79i, 1.95+0.79i) 3. OC (1.43+1.42i, 1.46+1.43i, 1.46+1.25i, 1.46+2.67i, 1.45+1.89i, 1.42+1.71i, 1.43+1.71i, 1.25+0.007i, 2.67+0.005i, 1.89+0.01i, 1.71+0.013i, 1.43+0.014i, 1.46+0.025i, 1.46+0.062i, 1.46+0.064i, 1.45+0.031i) 4. Salt (1.43+0.019i, 1.37+0.0043i, 1.36+0.0084i, 1.36+0.011i, 1.34+0.01i, 1.35+0.083i, 1.34+0.029i, 1.31+0.03i, 1.33+0.037i, 1.29+0.042i, 1.2+0.09i, 1.2+0.27i, 1.3+0.34i, 1.47+0.37i, 1.56+0.03i, 1.51+0.09i) 5. PPM (1.45+0.01i, 1.45+0.01i, 1.45+0.01i, 1.45+0.01i, 1.45+0.01i, 1.45+0.01i, 1.45+0.05i, 1+0.5i, 1+0.2i, 2.6+0.2i, 1.7+0.2i, 1.7+0.2i, 1.7+0.2i, 1.7+0.2i, 1.7+0.2i, 1.7+0.2i) 6. SOA (1.56+0.003i, 1.56+0.003i, 1.56+0.003i, 1.56+0.003i, 1.56+0.003i, 1.56+0.003i, 1.56+0.003i, 1.56+0.003i, 1.56+0.003i, 1.56+0.003i, 1.56+0.003i, 1.56+0.003i, 1.56+0.003i, 1.56+0.003i, 1.56+0.003i, 1.56+0.003i)

7. H_2SO_4 (1.35+0.16i, 1.4+0.13i, 1.39+0.12i, 1.38+0.12i, 1.35+0.15i, 1.42+0.18i, 1.26+0.16i, 1.15+0.44i, 1.57+0.73i, 1.83+0.7i, 1.71+0.46i, 1.68+0.2i, 1.59+0.21i, 1.87+0.48i, 1.89+0.27i, 1.86+0.31i)
8. HNO_3 (1.45+0.01i, 1.45+0.01i, 1.45+0.01i, 1.45+0.01i, 1.45+0.01i, 1.45+0.01i, 1.45+0.05i, 1+0.5i, 1+0.2i, 2.6+0.2i, 1.7+0.2i, 1.7+0.2i, 1.7+0.2i, 1.7+0.2i, 1.7+0.2i, 1.7+0.2i)
9. NH_3 (1.45+0.01i, 1.45+0.01i, 1.45+0.01i, 1.45+0.01i, 1.45+0.01i, 1.45+0.01i, 1.45+0.05i, 1+0.5i, 1+0.2i, 2.6+0.2i, 1.7+0.2i, 1.7+0.2i, 1.7+0.2i, 1.7+0.2i, 1.7+0.2i, 1.7+0.2i) in term of 16 wavelengths at 3.4, 4, 4.3, 4.6, 5.2, 6.1, 7.0, 7.8, 8.8, 9.7, 11.1, 13.2, 15.0, 17.7, 23.5, 55.6 μm

Table S7. Microphysics variables used in the two-way coupled WRF-CMAQ, WRF-Chem and WRF-CHIMERE models with enabling ACI effects compared to *those* without aerosol feedbacks.

Model	Microphysics scheme	Turning off feedback	Turning on ACI feedback	
			First indirect effects	Second indirect effects
WRF-CMAQ	Morrison	1. Prescribed constant CDNC value of 250 cm^{-3}	None	None
WRF-Chem	Morrison	1. Prescribed constant CDNC value of 250 cm^{-3} 2. Constant cloud droplet effective radius with 10 μm 3. Cloud droplet extinction coefficient, single scattering albedo, and asymmetry factor 4. Prescribed ice nucleating particle (INP) concentration based on empirical formula (Rasmussen et al., 2002)	1. Hygroscopicity 2. Prognostic CDNC based on Köhler theory 3. Prognostic cloud droplet effective radius 4. Prognostic cloud droplet extinction coefficient, single scattering albedo, and asymmetry factor 5. Prescribed INP	1. Prognostic cloud-to-rain autoconversion rate
WRF-CHIMERE	Thompson	1. Prescribed constant CDNC values of 300 cm^{-3} 2. Prescribed INP from heterogeneous ice nucleation in iceDeMott subroutine module_mp_thompson.F file using climatical dust concentration (dimeters > 0.5μm) (DeMott et al., 2015) and homogeneous freezing (Thompson and Eidhammer, 2014) with climatological hygroscopic aerosol concentrations (dimeters > 0.1μm) generated by QNWFA_QNIFA_Monthly_GFS file 3. Prescribed cloud droplet and ice effective radius 4. Prescribed extinction coefficient, single scattering albedo, and asymmetry factor of cloud droplet and ice	1. Hygroscopicity 2. Prognostic CDNC based on Köhler theory 3. Prognostic INP from heterogeneous ice nucleation based on online dust calculation (dimeters > 0.5 μm) and homogeneous freezing with prognostic hygroscopic aerosol concentrations (dimeters > 0.1μm) (Tuccella et al., 2019) 4. Prognostic cloud droplet and ice effective radius 5. Prognostic extinction coefficient, single scattering albedo, and asymmetry factor of cloud droplet and ice	1. Prognostic cloud-to-rain autoconversion rate

Table S8. Summary of download information on model output of each simulation scenario.

Scenario	DOI	Link	Reference
WRF-CMAQ_NO	https://doi.org/10.5281/zenodo.7951404	https://zenodo.org/record/7951404	Gao et al., 2023i_part1
	https://doi.org/10.5281/zenodo.7951467	https://zenodo.org/record/7951467	Gao et al., 2023i_part2
	https://doi.org/10.5281/zenodo.7951475	https://zenodo.org/record/7951475	Gao et al., 2023i_part3
WRF-CMAQ_ARI	https://doi.org/10.5281/zenodo.7949895	https://zenodo.org/record/7949895	Gao et al., 2023j_part1
	https://doi.org/10.5281/zenodo.7950644	https://zenodo.org/record/7950644	Gao et al., 2023j_part2
	https://doi.org/10.5281/zenodo.7950830	https://zenodo.org/record/7950830	Gao et al., 2023j_part3
WRF-Chem_NO	https://doi.org/10.5281/zenodo.7943804	https://zenodo.org/record/7943804	Gao et al., 2023k_part1
	https://doi.org/10.5281/zenodo.7945383	https://zenodo.org/record/7945383	Gao et al., 2023k_part2
	https://doi.org/10.5281/zenodo.7946944	https://zenodo.org/record/7946944	Gao et al., 2023k_part3
	https://doi.org/10.5281/zenodo.7947169	https://zenodo.org/record/7947169	Gao et al., 2023k_part4
WRF-Chem_ARI	https://doi.org/10.5281/zenodo.7947050	https://zenodo.org/record/7947050	Gao et al., 2023l_part1
	https://doi.org/10.5281/zenodo.7948216	https://zenodo.org/record/7948216	Gao et al., 2023l_part2
	https://doi.org/10.5281/zenodo.7949410	https://zenodo.org/record/7949410	Gao et al., 2023l_part3
	https://doi.org/10.5281/zenodo.7949561	https://zenodo.org/record/7949561	Gao et al., 2023l_part4
WRF-Chem_BOTH	https://doi.org/10.5281/zenodo.7939221	https://zenodo.org/record/7939221	Gao et al. 2023m_part1
	https://doi.org/10.5281/zenodo.7943002	https://zenodo.org/record/7943002	Gao et al. 2023m_part2
	https://doi.org/10.5281/zenodo.7943079	https://zenodo.org/record/7943079	Gao et al. 2023m_part3
	https://doi.org/10.5281/zenodo.7943323	https://zenodo.org/record/7943323	Gao et al. 2023m_part4
WRF-CHIMERE_NO	https://doi.org/10.5281/zenodo.7951775	https://zenodo.org/record/7951775	Gao et al. 2023n_part1
	https://doi.org/10.5281/zenodo.7951779	https://zenodo.org/record/7951779	Gao et al. 2023n_part2
	https://doi.org/10.5281/zenodo.7951791	https://zenodo.org/record/7951791	Gao et al. 2023n_part3
	https://doi.org/10.5281/zenodo.7951793	https://zenodo.org/record/7951793	Gao et al. 2023n_part4
WRF-CHIMERE_ARI	https://doi.org/10.5281/zenodo.7952838	https://zenodo.org/record/7952838	Gao et al. 2023o_part1
	https://doi.org/10.5281/zenodo.7952840	https://zenodo.org/record/7952840	Gao et al. 2023o_part2
	https://doi.org/10.5281/zenodo.7952842	https://zenodo.org/record/7952842	Gao et al. 2023o_part3
	https://doi.org/10.5281/zenodo.7952844	https://zenodo.org/record/7952844	Gao et al. 2023o_part4
WRF-CHIMERE_BOTH	https://doi.org/10.5281/zenodo.7952859	https://zenodo.org/record/7952859	Gao et al. 2023p_part1
	https://doi.org/10.5281/zenodo.7952863	https://zenodo.org/record/7952863	Gao et al. 2023p_part2
	https://doi.org/10.5281/zenodo.7952865	https://zenodo.org/record/7952865	Gao et al. 2023p_part3
	https://doi.org/10.5281/zenodo.7952867	https://zenodo.org/record/7952867	Gao et al. 2023p_part4

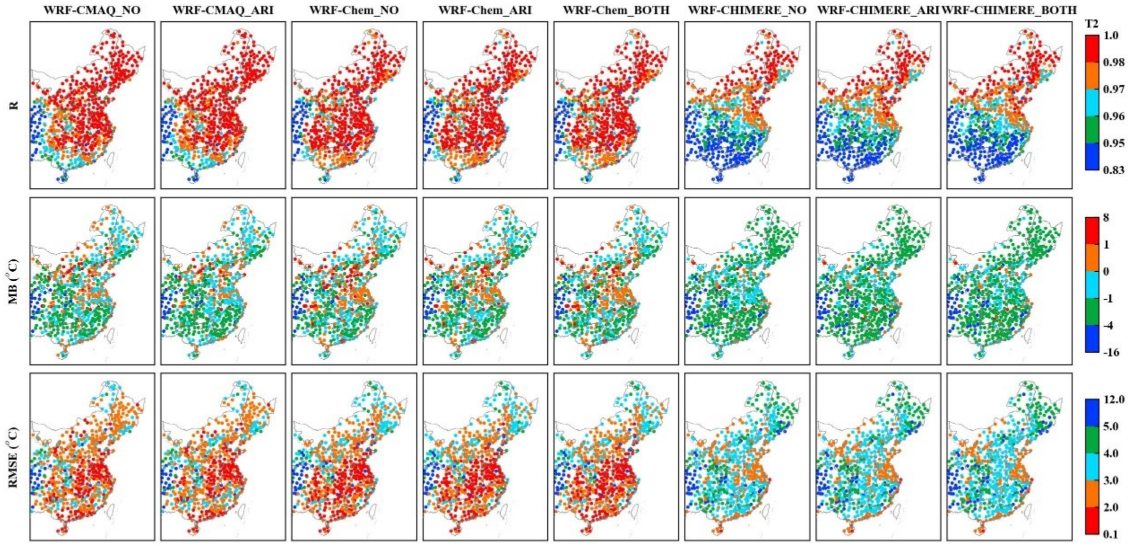

Figure S1. Statistical metrics (R, MB and RMSE) between simulated and observed annual T2 in eastern China.

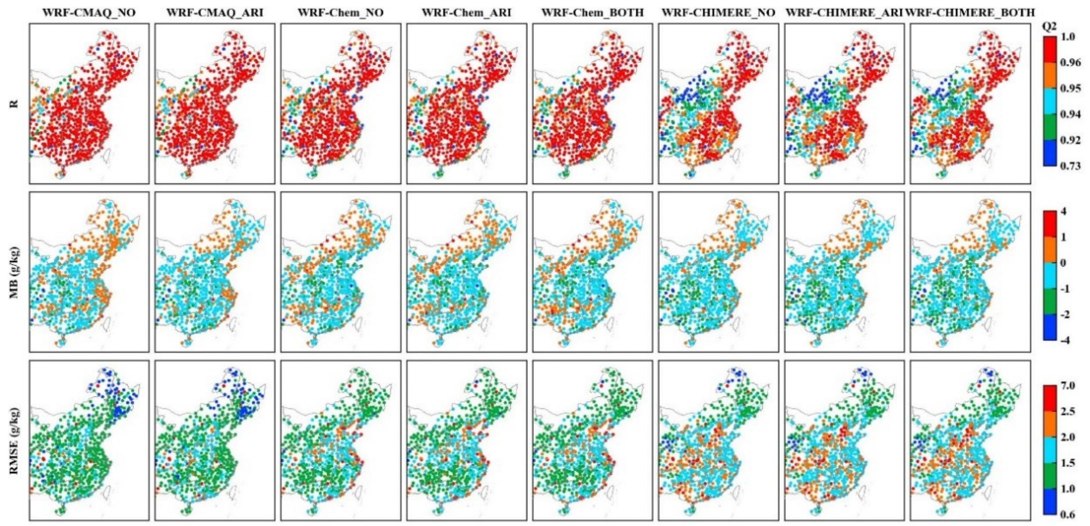

Figure S2. The same as Fig. S1 but for Q2.

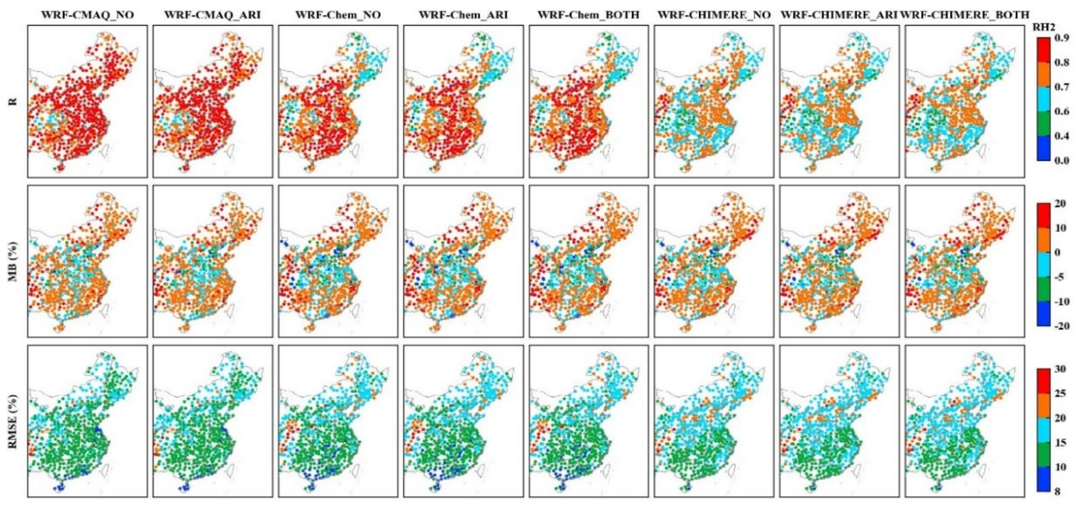

Figure S3. The same as Fig. S1 but for RH2.

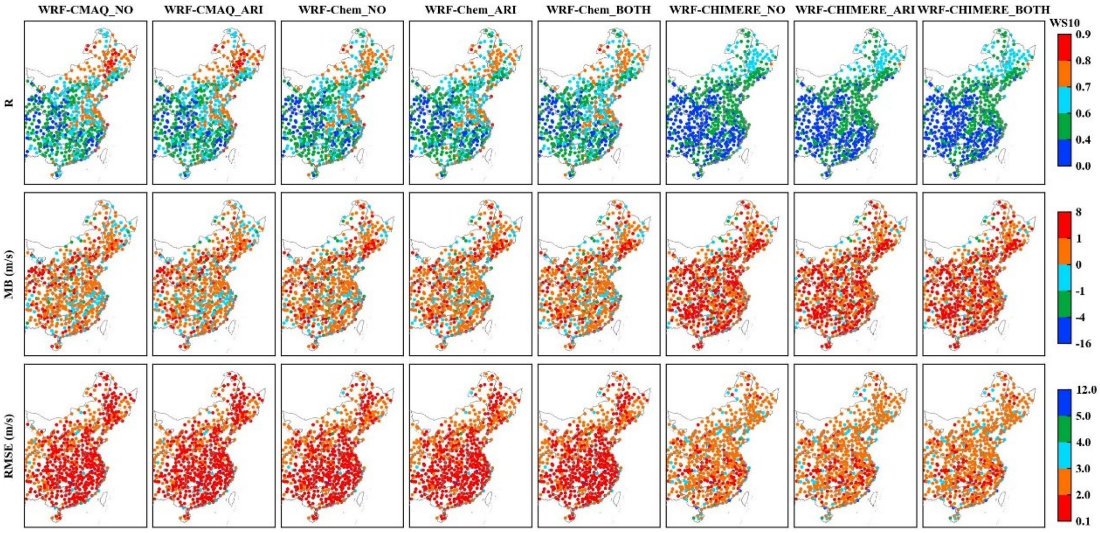

Figure S4. The same as Fig. S1 but for WS10.

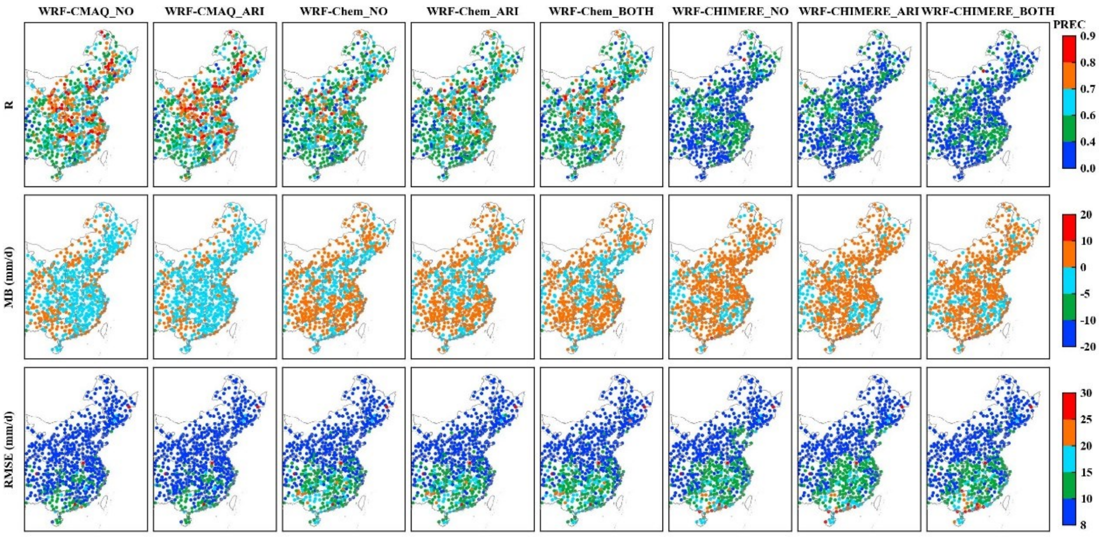

Figure S5. The same as Fig. S1 but for PREC.

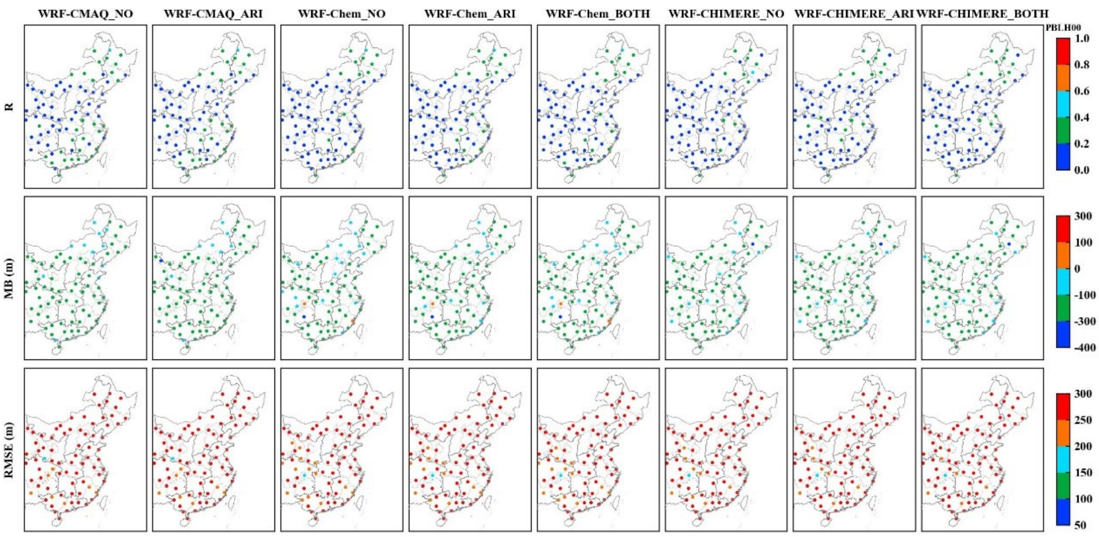

Figure S6. The same as Fig. S1 but for PBLH at 08:00 LT.

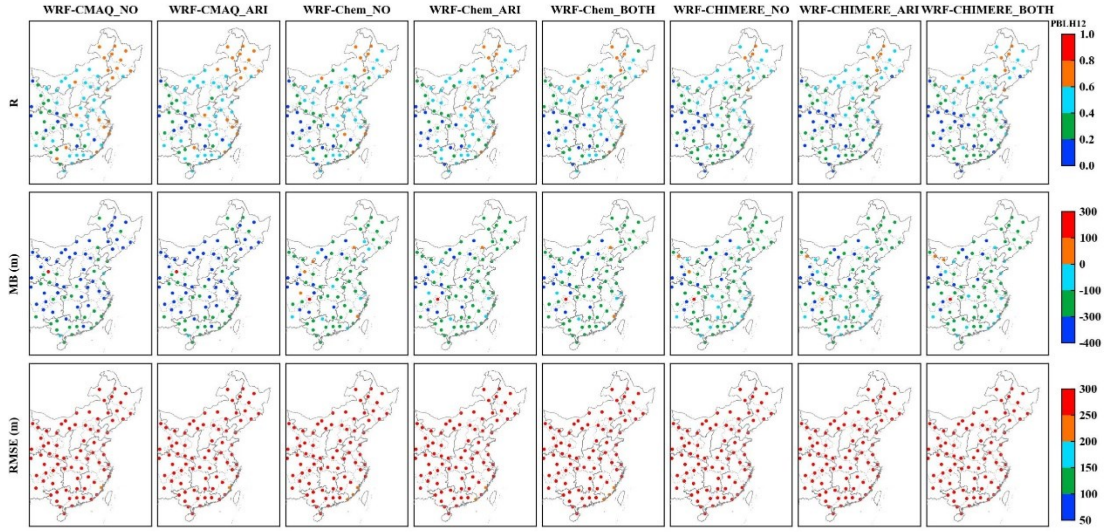

Figure S7. The same as Fig. S1 but for PBLH at 20:00 LT.

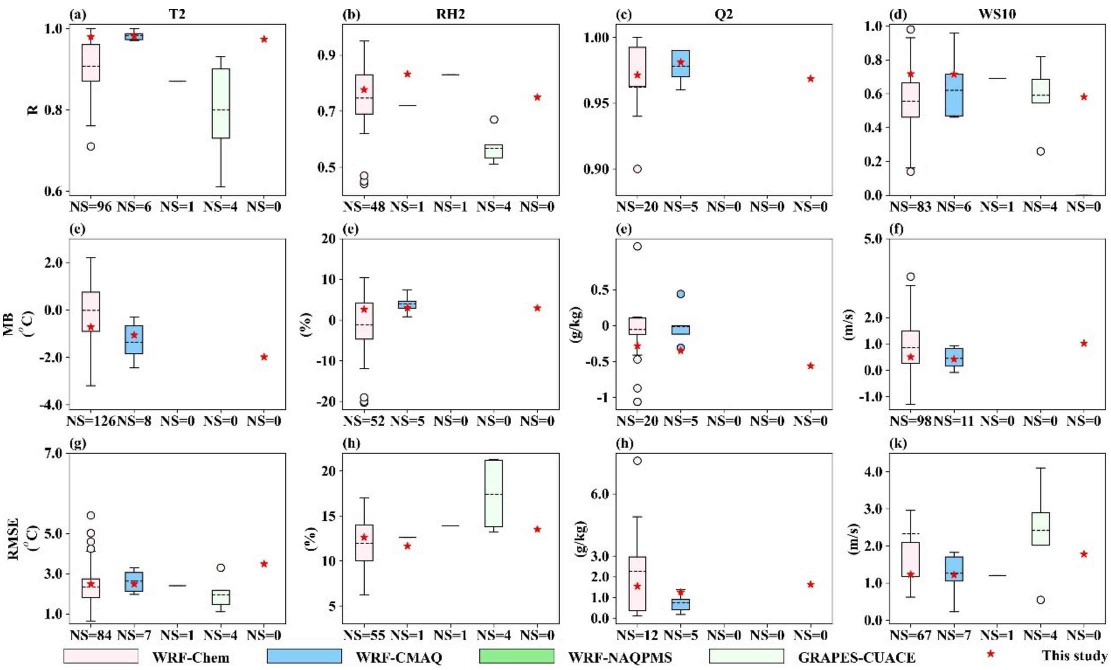

Figure S8. Comparisons of model capacities between our study (red stars) and previous literature (box plots) in terms of the surface T2, RH2, Q2, and WS10 in eastern China. Note that red stars in the fifth column of each subgraph represent the statistical metrics of WRF-CHIMERE in this study.

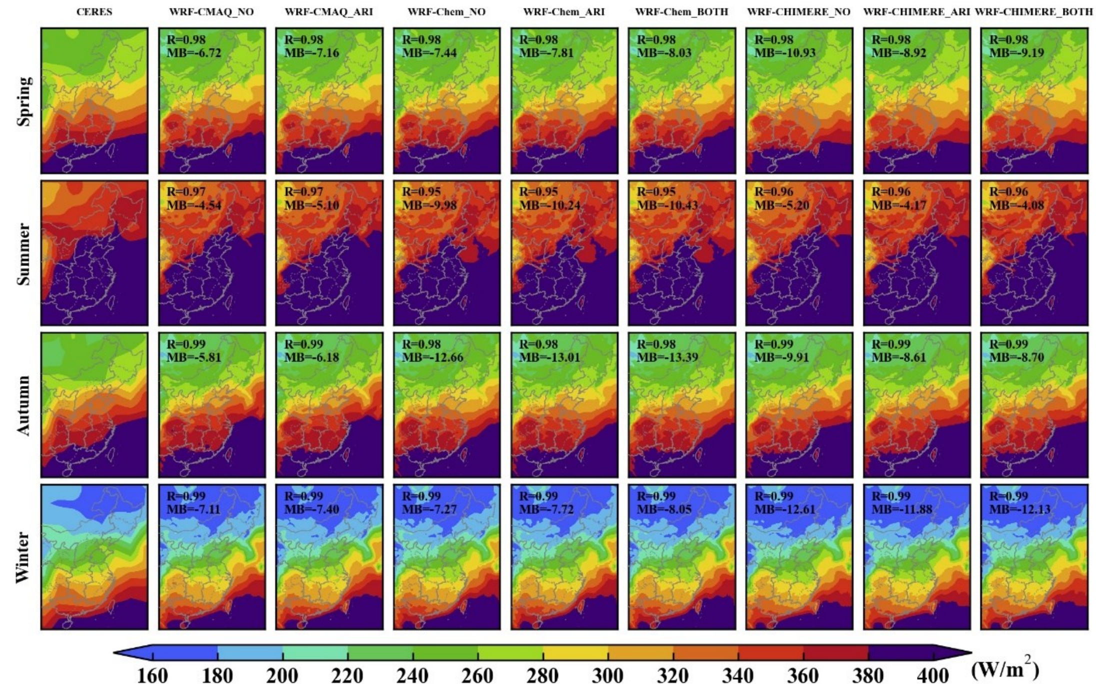

Figure S9. Spatial distributions of seasonal SLR between CERES observations and simulations from WRF-CMAQ, WRF-Chem, and WRF-CHIMERE with and without aerosol feedbacks in eastern China.

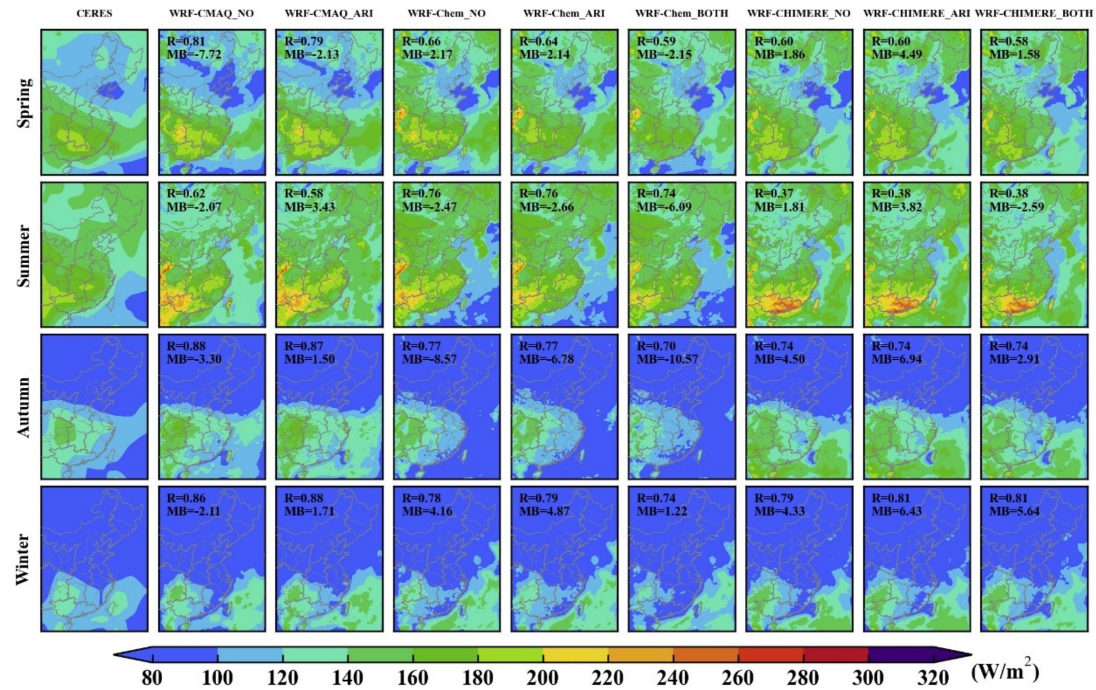

Figure S10. The same as Fig. S9 but for SRTOA.

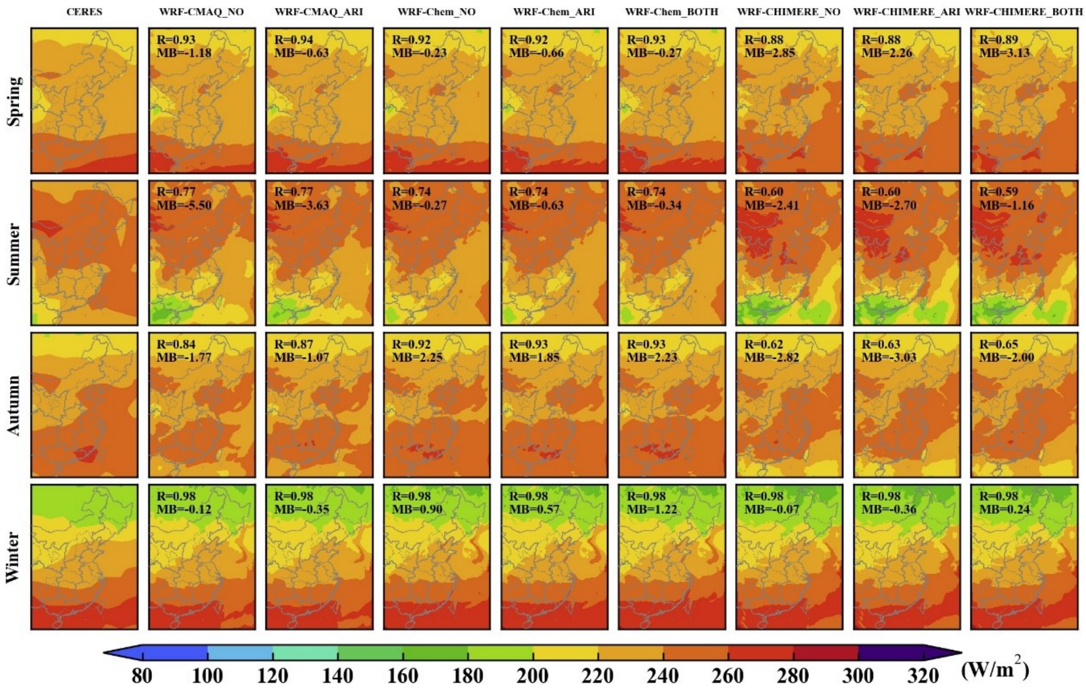

Figure S11. The same as Fig. S9 but for LRTOA.

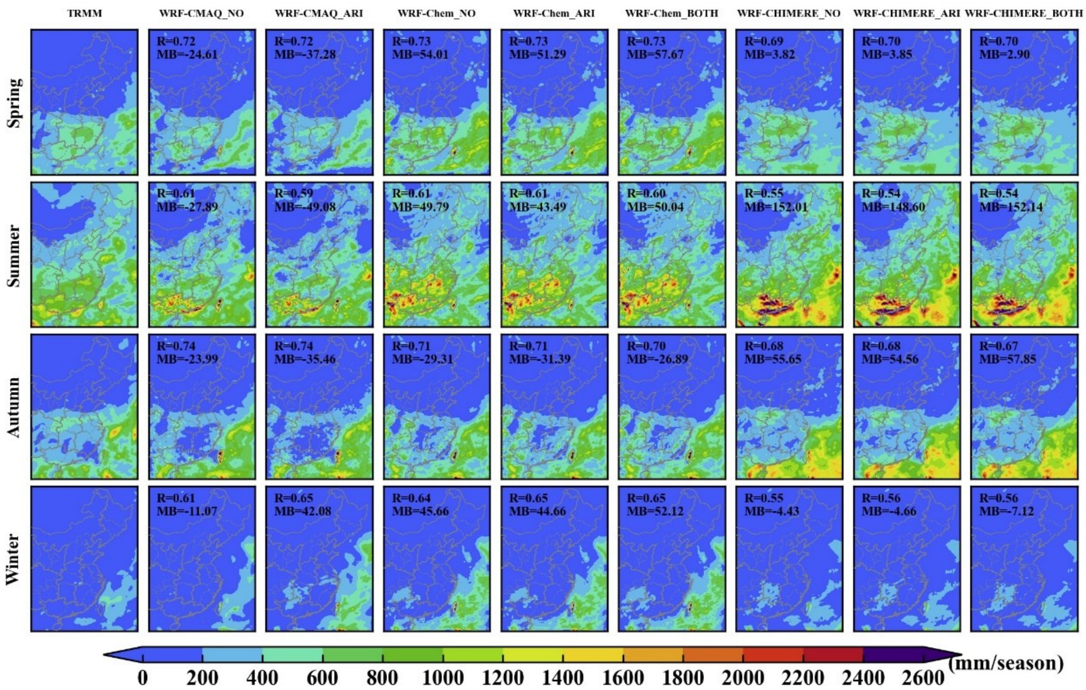

Figure S12. The same as Fig. S9 but for precipitation.

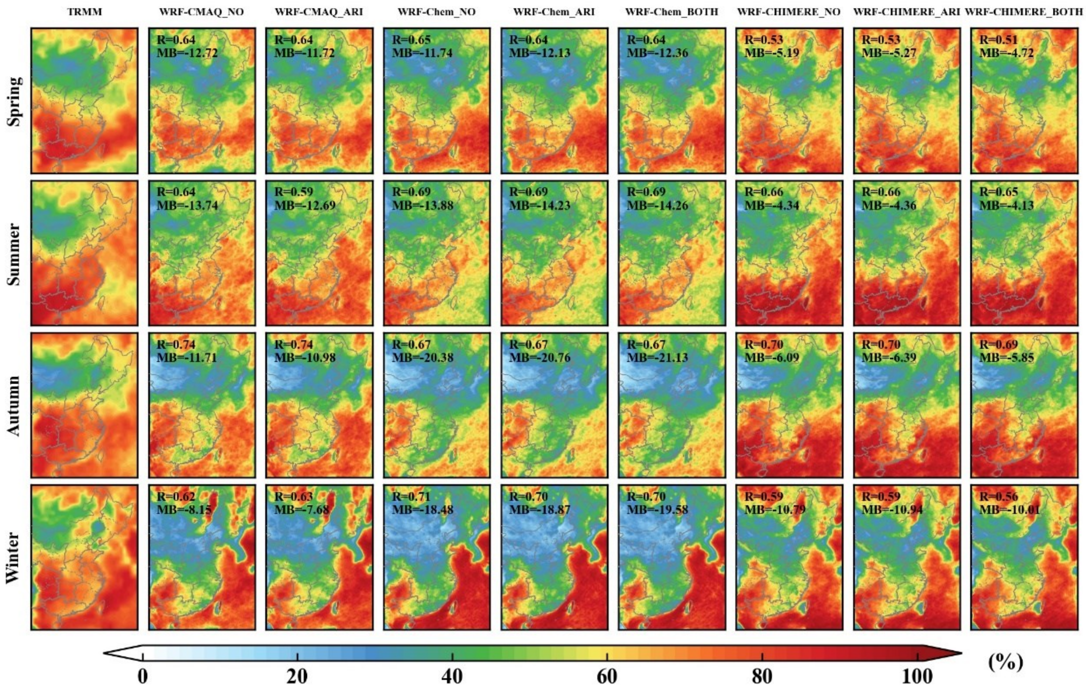

Figure S13. The same as Fig. S9 but for cloud fraction.

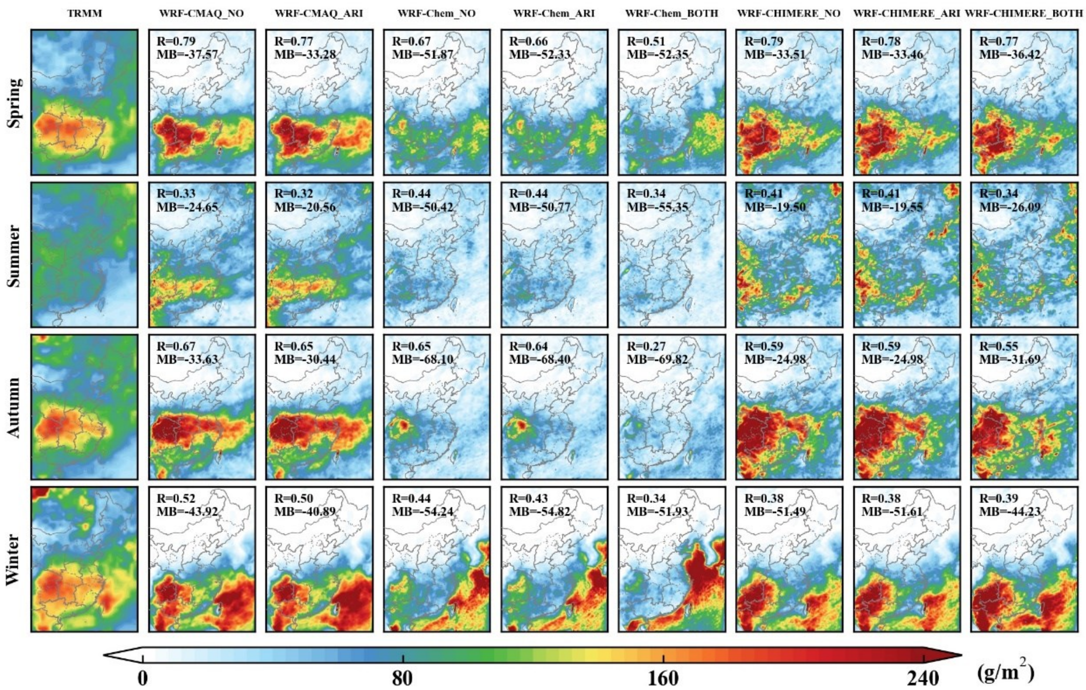

Figure S14. The same as Fig. S9 but for liquid water path.

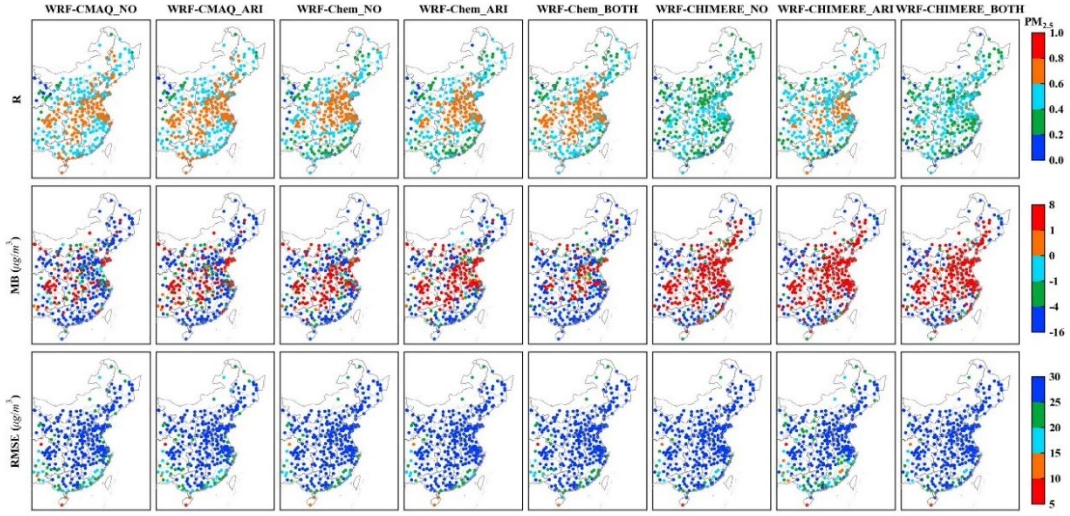

Figure S15. Statistical metrics (R, MB and RMSE) between simulated and observed annual $PM_{2.5}$ concentrations in eastern China.

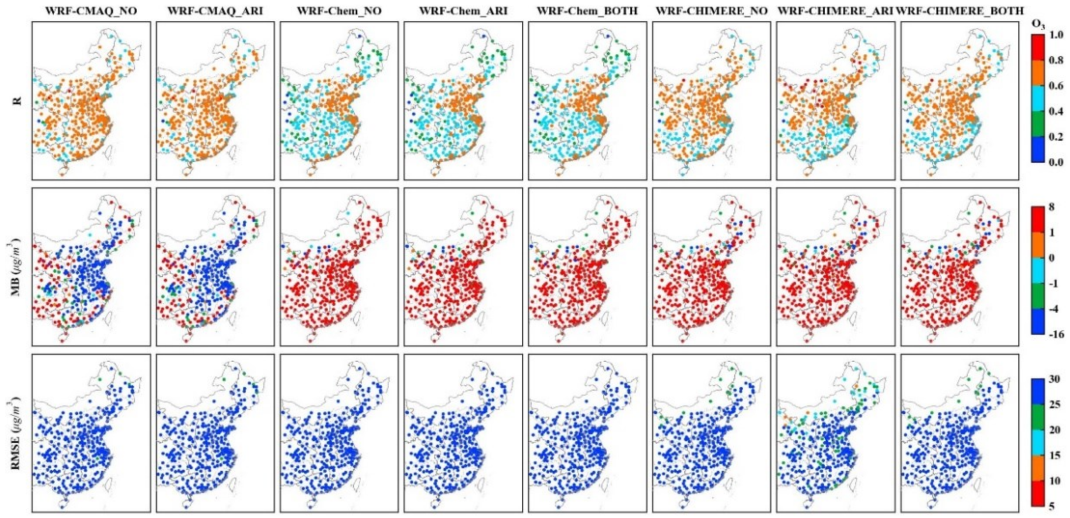

Figure S16. The same as Fig. S15 but for O_3.

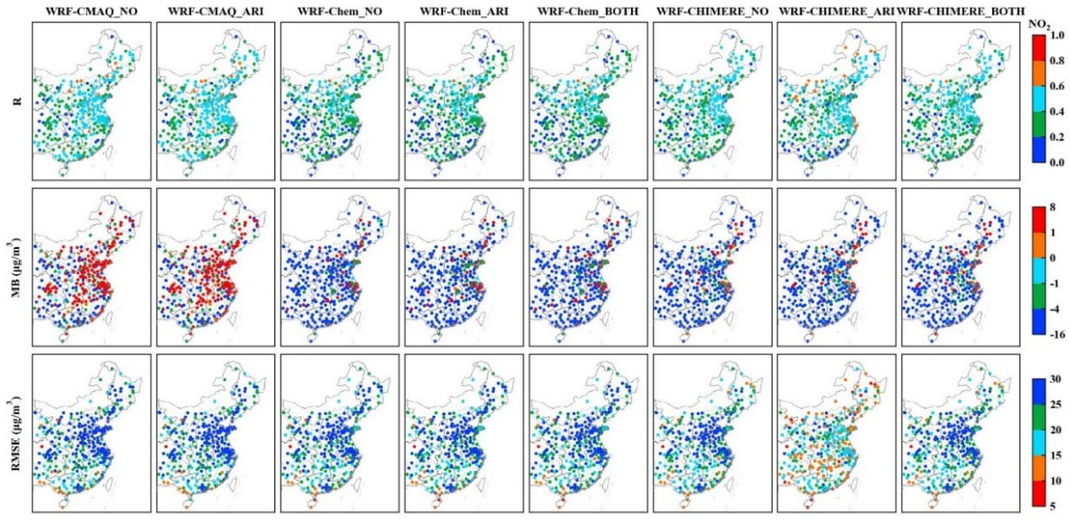

Figure S17. The same as Fig. S15 but for NO_2.

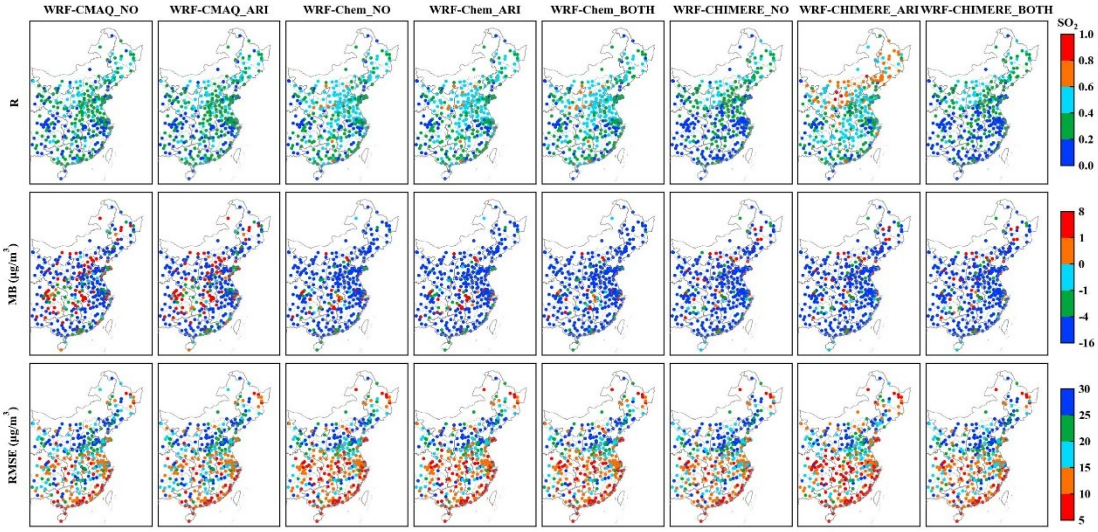

Figure S18. The same as Fig. S15 but for SO_2.

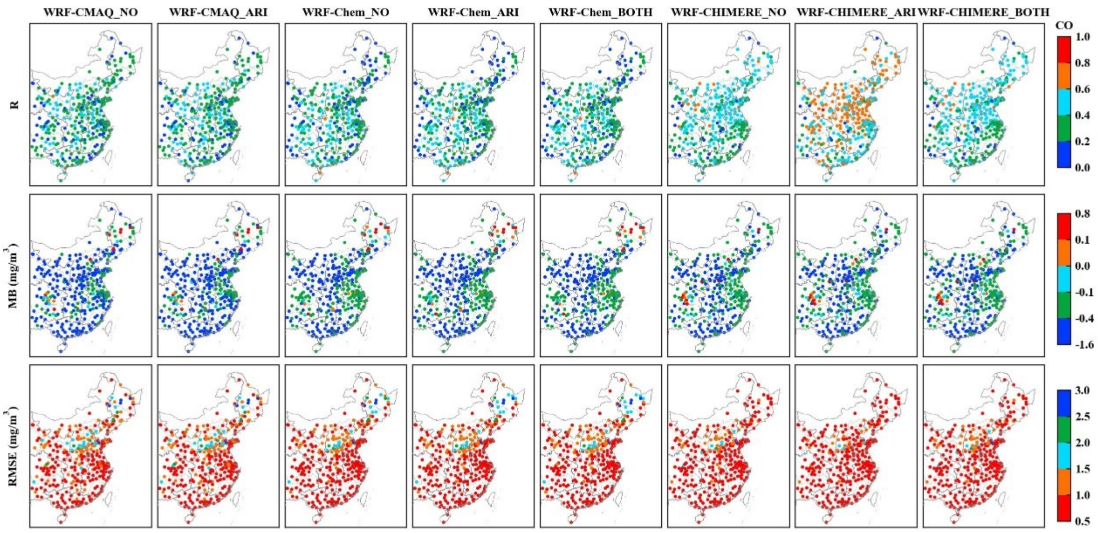

Figure S19. The same as Fig. S15 but for CO.

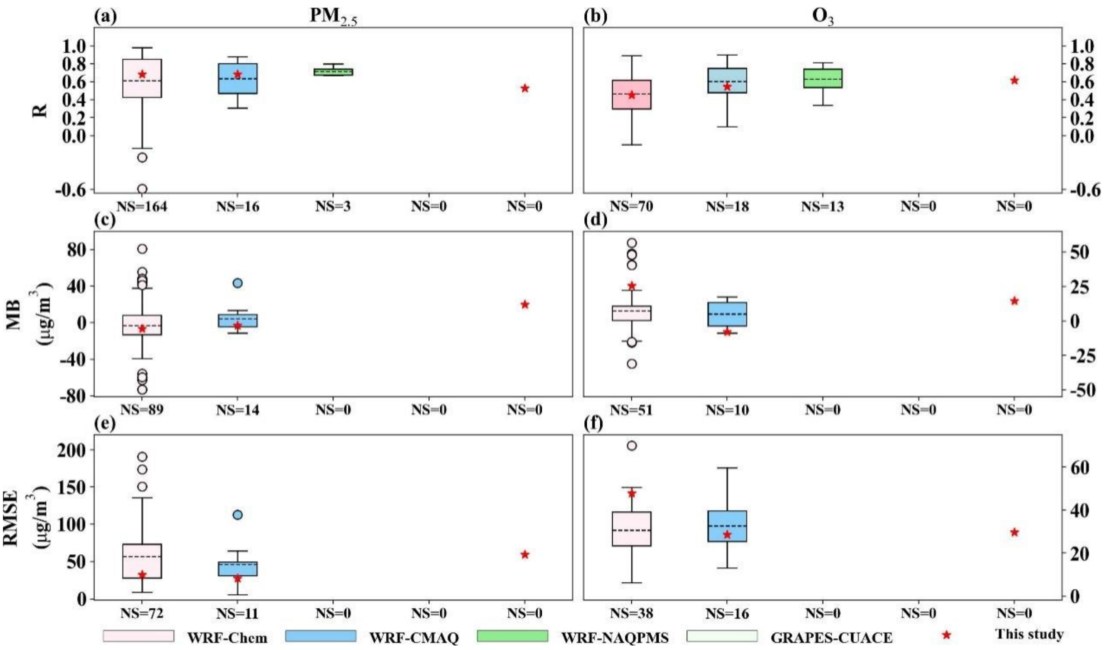

Figure S20. Comparisons of model capacities between our study (red stars) and previous literature (box plots) in terms of surface $PM_{2.5}$ and O_3 concentrations in eastern China. Note that red stars in the fifth column of each subgraph represent the statistical metrics of WRF-CHIMERE in this study.

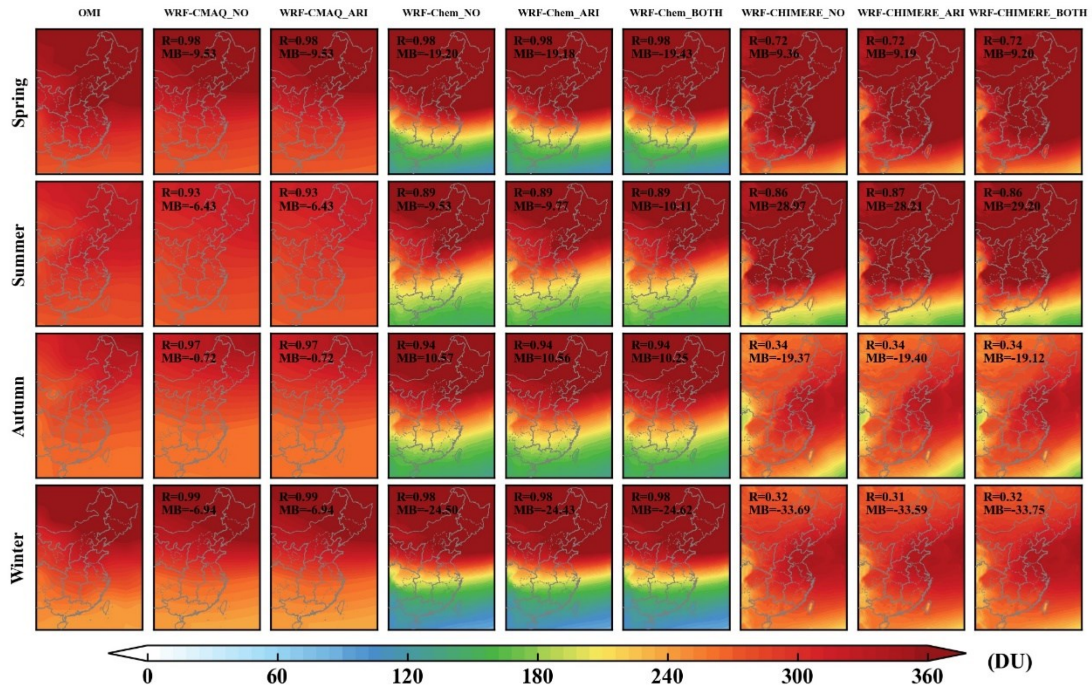

Figure S21. Spatial distributions of seasonal total column ozone between OMI observations and simulations from WRF-CMAQ, WRF-Chem and WRF-CHIMERE with and without aerosol feedbacks in eastern China.

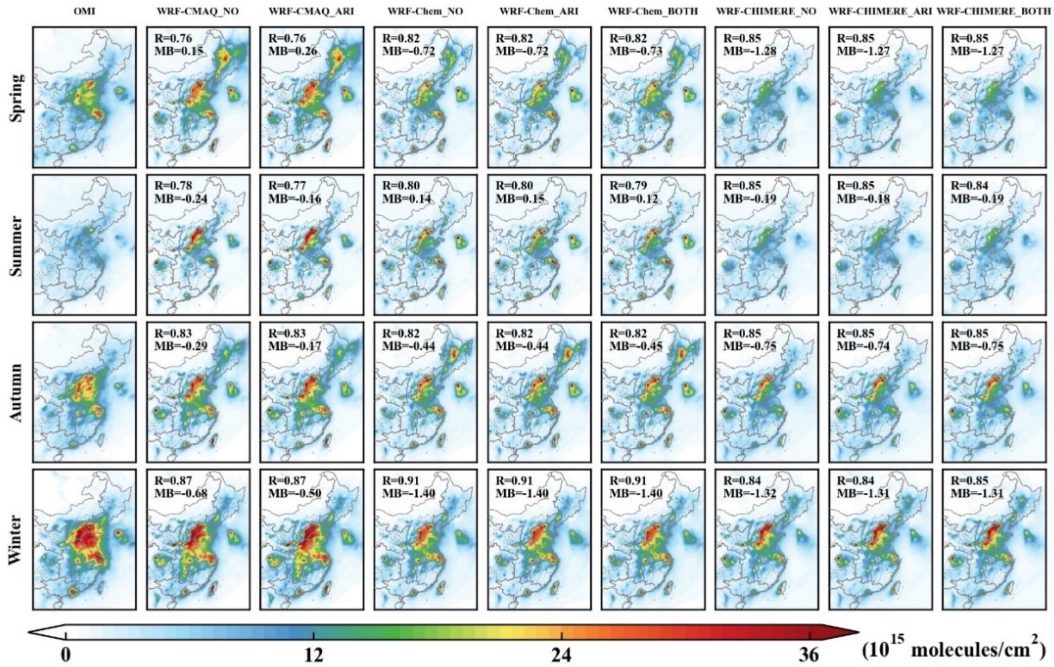

Figure S22. The same as Fig. S21 but for tropospheric NO_2 column.

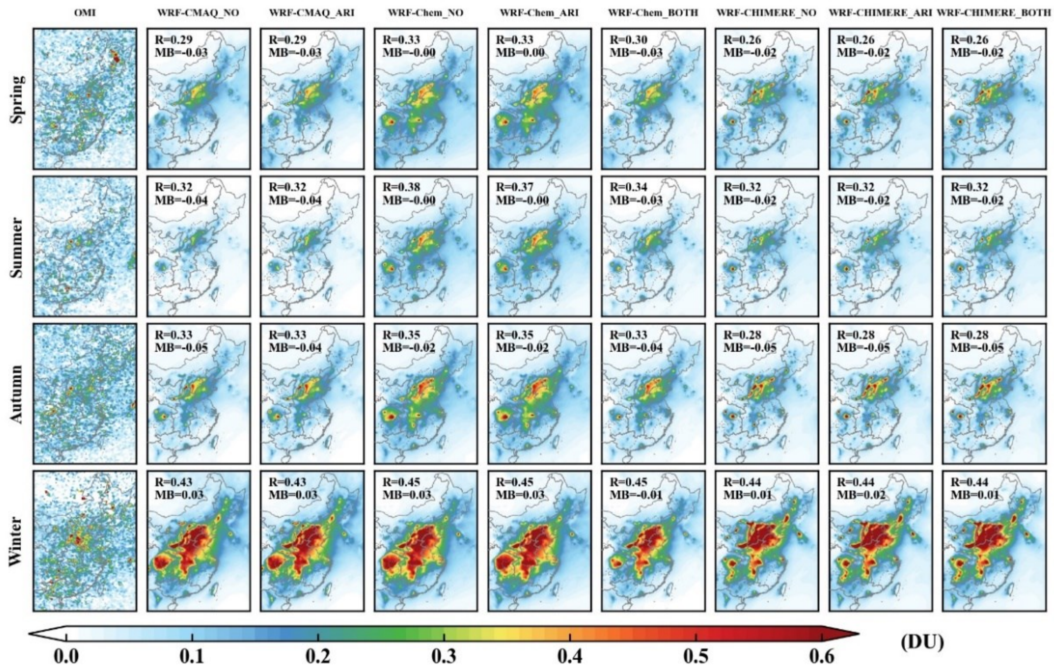

Figure S23. The same as Fig. S21 but for PBL SO_2 column.

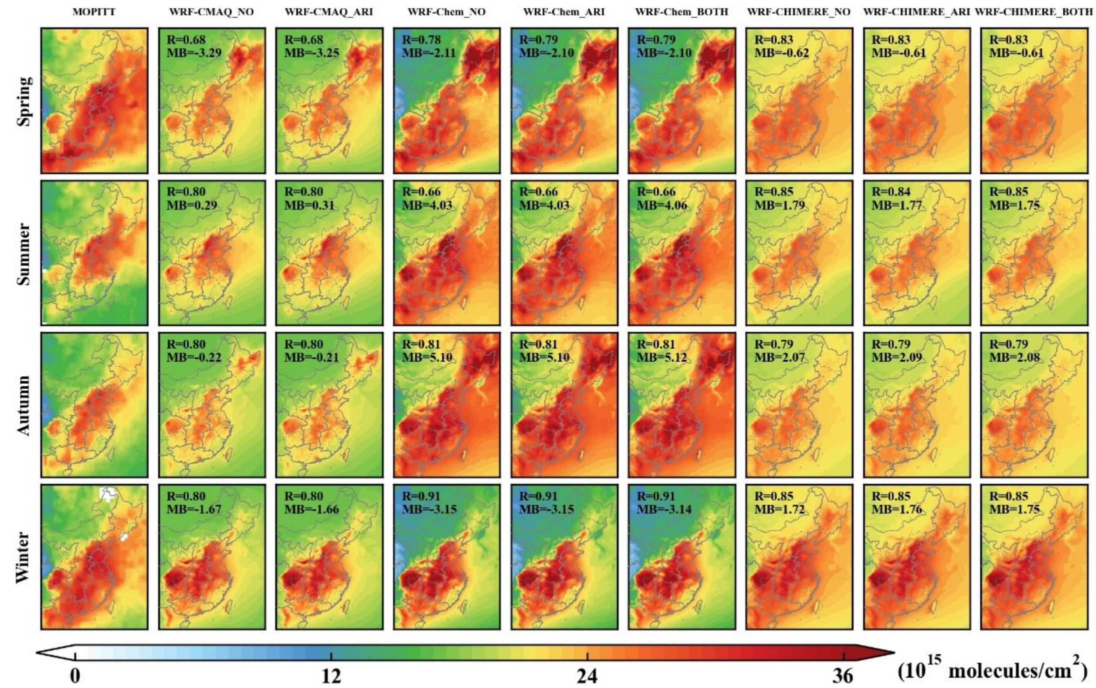

Figure S24. The same as Fig. S21 but for total CO column concentrations.

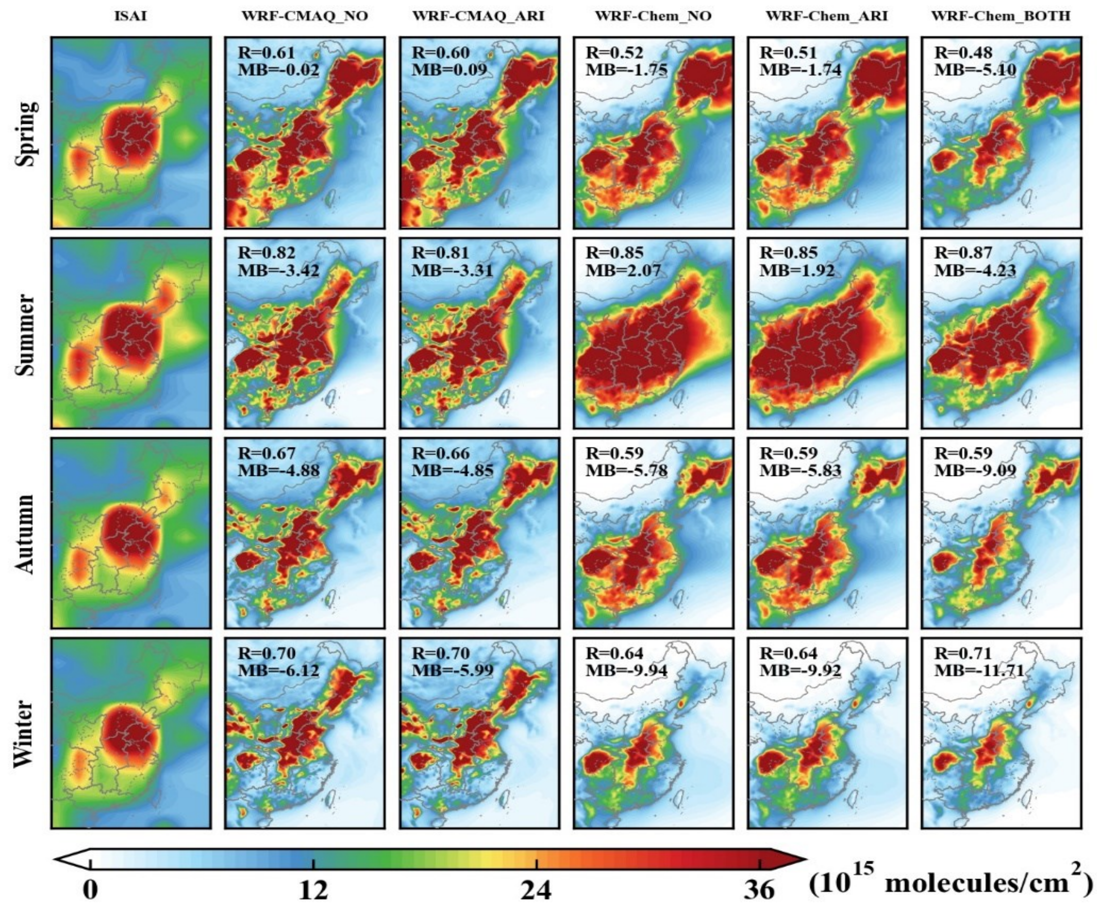

Figure S25. Spatial distributions of seasonal total NH_3 column between MOPITT observations and simulations from WRF-CMAQ and WRF-Chem with and without aerosol feedbacks in eastern China.

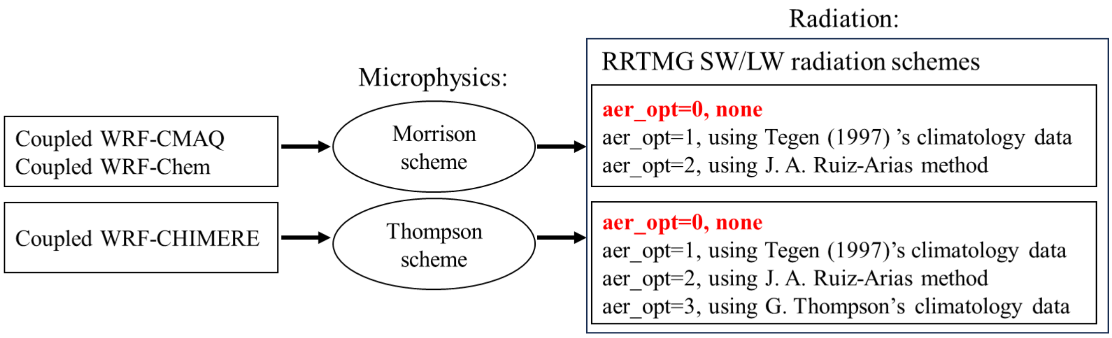

Figure S26. Summary of the selected options of radiation and microphysics schemes in coupled WRF-CMAQ, WRF-Chem and WRF-CHIMERE in this study.

Reference

Briant, R., Tuccella, P., Deroubaix, A., Khvorostyanov, D., Menut, L., Mailler, S., and Turquety, S.: Aerosol-radiation interaction modelling using online coupling between the WRF 3.7.1 meteorological model and the CHIMERE 2016 chemistry-transport model, through the OASIS3-MCT coupler, Geoscientific Model Development, 10, 927–944, https://doi.org/10.5194/gmd-10-927-2017, 2017.

Brunner, D., Savage, N., Jorba, O., Eder, B., Giordano, L., Badia, A., Balzarini, A., Baro, R., Bianconi, R., and Chemel, C.: Comparative analysis of meteorological performance of coupled chemistry-meteorology models in the context of AQMEII phase 2, Atmos. Environ., 115, 470–498, https://doi.org/10.1016/j.atmosenv.2014.12.032, 2015.

Chao Gao, Xuelei Zhang, Aijun Xiu, Qingqing Tong, Hongmei Zhao, Shichun Zhang, Guangyi Yang, Mengduo Zhang, Shengjin Xie: Simulation results from WRF-CMAQ without aerosol feedbacks in eastern China for January-April 2017, Zenodo [data set], https://doi.org/10.5281/zenodo.7951404, 2023i_part1.

Chao Gao, Xuelei Zhang, Aijun Xiu, Qingqing Tong, Hongmei Zhao, Shichun Zhang, Guangyi Yang, Mengduo Zhang, Shengjin Xie: Simulation results from WRF-CMAQ without aerosol feedbacks in eastern China for May-August 2017, Zenodo [data set], https://doi.org/10.5281/zenodo.7951467, 2023i_part2.

Chao Gao, Xuelei Zhang, Aijun Xiu, Qingqing Tong, Hongmei Zhao, Shichun Zhang, Guangyi Yang, Mengduo Zhang, Shengjin Xie: Simulation results from WRF-CMAQ without aerosol feedbacks in eastern China for September-December 2017, Zenodo [data set], https://doi.org/10.5281/zenodo.7951475, 2023i_part3.

Chao Gao, Xuelei Zhang, Aijun Xiu, Qingqing Tong, Hongmei Zhao, Shichun Zhang, Guangyi Yang, Mengduo Zhang, Shengjin Xie: Simulation results from WRF-CMAQ with enabling aerosol-radiation interactions in eastern China for January-April 2017, Zenodo [data set], https://doi.org/10.5281/zenodo.7949895, 2023j_part1.

Chao Gao, Xuelei Zhang, Aijun Xiu, Qingqing Tong, Hongmei Zhao, Shichun Zhang, Guangyi Yang, Mengduo Zhang, Shengjin Xie: Simulation results from WRF-CMAQ with enabling aerosol-radiation interactions in eastern China for May-August 2017, Zenodo [data set], https://doi.org/10.5281/zenodo.7950644, 2023j_part2.

Chao Gao, Xuelei Zhang, Aijun Xiu, Qingqing Tong, Hongmei Zhao, Shichun Zhang, Guangyi Yang, Mengduo Zhang, Shengjin Xie: Simulation results from WRF-CMAQ with enabling aerosol-radiation interactions in eastern China for September-December 2017, Zenodo [data set], https://doi.org/10.5281/zenodo.7950830, 2023j_part3.

Chao Gao, Xuelei Zhang, Aijun Xiu, Qingqing Tong, Hongmei Zhao, Shichun Zhang, Guangyi Yang, Mengduo Zhang, Shengjin Xie: Simulation results from WRF-Chem without aerosol feedbacks in eastern China for January-March 2017, Zenodo [data set], https://doi.org/10.5281/zenodo.7943804, 2023k_part1.

Chao Gao, Xuelei Zhang, Aijun Xiu, Qingqing Tong, Hongmei Zhao, Shichun Zhang, Guangyi Yang, Mengduo Zhang, Shengjin Xie: Simulation results from WRF-Chem without aerosol feedbacks in eastern China for April-June 2017, Zenodo [data set], https://doi.org/10.5281/zenodo.7945383, 2023k_part2.

Chao Gao, Xuelei Zhang, Aijun Xiu, Qingqing Tong, Hongmei Zhao, Shichun Zhang, Guangyi Yang, Mengduo Zhang, Shengjin Xie: Simulation results from WRF-Chem without aerosol feedbacks in eastern China for July-September 2017, Zenodo [data set], https://doi.org/10.5281/zenodo.7946944, 2023k_part3.

Chao Gao, Xuelei Zhang, Aijun Xiu, Qingqing Tong, Hongmei Zhao, Shichun Zhang, Guangyi Yang, Mengduo Zhang, Shengjin Xie: Simulation results from WRF-Chem without aerosol feedbacks in eastern China for October-December 2017, Zenodo [data set], https://doi.org/10.5281/zenodo.7947169, 2023k_part4.

Chao Gao, Xuelei Zhang, Aijun Xiu, Qingqing Tong, Hongmei Zhao, Shichun Zhang, Guangyi Yang, Mengduo Zhang, Shengjin Xie: Simulation results from WRF-Chem with enabling aerosol-radiation interactions in eastern China for January-March 2017, Zenodo [data set], https://doi.org/10.5281/zenodo.7947050, 2023l_part1.

Chao Gao, Xuelei Zhang, Aijun Xiu, Qingqing Tong, Hongmei Zhao, Shichun Zhang, Guangyi Yang, Mengduo Zhang, Shengjin Xie: Simulation results from WRF-Chem with enabling aerosol-radiation interactions in eastern China for April-June 2017, Zenodo [data set], https://doi.org/10.5281/zenodo.7948216, 2023l_part2.

Chao Gao, Xuelei Zhang, Aijun Xiu, Qingqing Tong, Hongmei Zhao, Shichun Zhang, Guangyi Yang, Mengduo Zhang, Shengjin Xie: Simulation results from WRF-Chem with enabling aerosol-radiation interactions in eastern China for July-September 2017, Zenodo [data set], https://doi.org/10.5281/zenodo.7949410, 2023l_part3.

Chao Gao, Xuelei Zhang, Aijun Xiu, Qingqing Tong, Hongmei Zhao, Shichun Zhang, Guangyi Yang, Mengduo Zhang, Shengjin Xie: Simulation results from WRF-Chem with enabling aerosol-radiation interactions in eastern China for October-December 2017, Zenodo [data set], https://doi.org/10.5281/zenodo.7949561, 2023l_part4.

Chao Gao, Xuelei Zhang, Aijun Xiu, Qingqing Tong, Hongmei Zhao, Shichun Zhang, Guangyi Yang, Mengduo Zhang, Shengjin Xie: Simulation results from WRF-Chem with enabling aerosol-radiation interactions and aerosol-cloud interactions in eastern China for January-March 2017, Zenodo [data set], https://doi.org/10.5281/zenodo.7939221, 2023m_part1.

Chao Gao, Xuelei Zhang, Aijun Xiu, Qingqing Tong, Hongmei Zhao, Shichun Zhang, Guangyi Yang, Mengduo Zhang, Shengjin Xie: Simulation results from WRF-Chem with enabling aerosol-radiation interactions and aerosol-cloud interactions in eastern China for April-June 2017, Zenodo [data set], https://doi.org/10.5281/zenodo.7943002, 2023m_part2.

Chao Gao, Xuelei Zhang, Aijun Xiu, Qingqing Tong, Hongmei Zhao, Shichun Zhang, Guangyi Yang, Mengduo Zhang, Shengjin Xie: Simulation results from WRF-Chem with enabling aerosol-radiation interactions and aerosol-cloud interactions in eastern China for July-September 2017, Zenodo [data set], https://doi.org/10.5281/zenodo.7943079, 2023m_part3.

Chao Gao, Xuelei Zhang, Aijun Xiu, Qingqing Tong, Hongmei Zhao, Shichun Zhang, Guangyi Yang, Mengduo Zhang, Shengjin Xie: Simulation results from WRF-Chem with enabling aerosol-radiation interactions and aerosol-cloud interactions in eastern China for October-December 2017, Zenodo [data set], https://doi.org/10.5281/zenodo.7943323, 2023m_part4.

Chao Gao, Xuelei Zhang, Aijun Xiu, Qingqing Tong, Hongmei Zhao, Shichun Zhang, Guangyi Yang, Mengduo Zhang, Shengjin Xie: Simulation results from WRF-CHIMERE without aerosol feedbacks in eastern China for January-March 2017, Zenodo [data set], https://doi.org/10.5281/zenodo.7951775, 2023n_part1.

Chao Gao, Xuelei Zhang, Aijun Xiu, Qingqing Tong, Hongmei Zhao, Shichun Zhang, Guangyi Yang, Mengduo Zhang, Shengjin Xie: Simulation results from WRF-CHIMERE without aerosol feedbacks in eastern China for April-June 2017, Zenodo [data set], https://doi.org/10.5281/zenodo.7951779, 2023n_part2.

Chao Gao, Xuelei Zhang, Aijun Xiu, Qingqing Tong, Hongmei Zhao, Shichun Zhang, Guangyi Yang, Mengduo Zhang, Shengjin Xie: Simulation results from WRF-CHIMERE without aerosol feedbacks in eastern China for July-September 2017, Zenodo [data set], https://doi.org/10.5281/zenodo.7951791, 2023n_part3.

Chao Gao, Xuelei Zhang, Aijun Xiu, Qingqing Tong, Hongmei Zhao, Shichun Zhang, Guangyi Yang, Mengduo Zhang, Shengjin Xie: Simulation results from WRF-CHIMERE without aerosol feedbacks in eastern China for October-December 2017, Zenodo [data set], https://doi.org/10.5281/zenodo.7951793, 2023n_part4.

Chao Gao, Xuelei Zhang, Aijun Xiu, Qingqing Tong, Hongmei Zhao, Shichun Zhang, Guangyi Yang, Mengduo Zhang, Shengjin Xie: Simulation results from WRF-CHIMERE with enabling aerosol-radiation interactions in eastern China for January-March 2017, Zenodo [data set], https://doi.org/10.5281/zenodo.7952838, 2023o_part1.

Chao Gao, Xuelei Zhang, Aijun Xiu, Qingqing Tong, Hongmei Zhao, Shichun Zhang, Guangyi Yang, Mengduo Zhang, Shengjin Xie: Simulation results from WRF-CHIMERE with enabling aerosol-radiation interactions in eastern China for April-June 2017, Zenodo [data set], https://doi.org/10.5281/zenodo.7952840, 2023o_part2.

Chao Gao, Xuelei Zhang, Aijun Xiu, Qingqing Tong, Hongmei Zhao, Shichun Zhang, Guangyi Yang, Mengduo Zhang, Shengjin Xie: Simulation results from WRF-CHIMERE with enabling aerosol-radiation interactions in eastern China for July-September 2017, Zenodo [data set], https://doi.org/10.5281/zenodo.7952842, 2023o_part3.

Chao Gao, Xuelei Zhang, Aijun Xiu, Qingqing Tong, Hongmei Zhao, Shichun Zhang, Guangyi Yang, Mengduo Zhang, Shengjin Xie: Simulation results from WRF-CHIMERE with enabling aerosol-radiation interactions in eastern China for October-December 2017, Zenodo [data set], https://doi.org/10.5281/zenodo.7952844, 2023o_part4.

Chao Gao, Xuelei Zhang, Aijun Xiu, Qingqing Tong, Hongmei Zhao, Shichun Zhang, Guangyi Yang, Mengduo Zhang, Shengjin Xie: Simulation results from WRF-CHIMERE with enabling aerosol-radiation interactions and aerosol-cloud interactions in eastern China for January-March 2017, Zenodo [data set], https://doi.org/10.5281/zenodo.7952859, 2023p_part1.

Chao Gao, Xuelei Zhang, Aijun Xiu, Qingqing Tong, Hongmei Zhao, Shichun Zhang, Guangyi Yang, Mengduo Zhang, Shengjin Xie: Simulation results from WRF-CHIMERE with enabling aerosol-radiation interactions and aerosol-cloud interactions in eastern China for April-June 2017, Zenodo [data set], https://doi.org/10.5281/zenodo.7952863, 2023p_part2.

Chao Gao, Xuelei Zhang, Aijun Xiu, Qingqing Tong, Hongmei Zhao, Shichun Zhang, Guangyi Yang, Mengduo Zhang, Shengjin Xie: Simulation results from WRF-CHIMERE with enabling aerosol-radiation interactions and aerosol-cloud interactions in eastern China for July-September 2017, Zenodo [data set], https://doi.org/10.5281/zenodo.7952865, 2023p_part3.

Chao Gao, Xuelei Zhang, Aijun Xiu, Qingqing Tong, Hongmei Zhao, Shichun Zhang, Guangyi Yang, Mengduo Zhang, Shengjin Xie: Simulation results from WRF-CHIMERE with enabling aerosol-radiation interactions and aerosol-cloud interactions in eastern China for October-December 2017, Zenodo [data set], https://doi.org/10.5281/zenodo.7952867, 2023p_part4.

DeMott, P. J., Prenni, A. J., McMeeking, G. R., Sullivan, R. C., Petters, M. D., Tobo, Y., Niemand, M., Möhler, O., Snider, J. R., Wang, Z., and Kreidenweis, S. M.: Integrating laboratory and field data to quantify the immersion freezing ice nucleation activity of mineral dust particles, Atmos. Chem. Phys., 15, 393–409, https://doi.org/10.5194/acp-15-393-2015, 2015.

Fu, Q.: An accurate parameterization of the solar radiative properties of cirrus clouds for climate models, Journal of climate, 9, 2058–2082, https://doi.org/10.1175/1520-0442(1996)009<2058:AAPOTS>2.0.CO;2, 1996.

Gao, M., Han, Z., Liu, Z., Li, M., Xin, J., Tao, Z., Li, J., Kang, J. E., Huang, K., Dong, X., Zhuang, B., Li, S., Ge, B., Wu, Q., Cheng, Y., Wang, Y., Lee, H. J., Kim, C. H., Fu, J. S., Wang, T., Chin, M., Woo, J. H., Zhang, Q., Wang, Z., and Carmichael, G. R.: Air quality and climate change, Topic 3 of the Model Inter-Comparison Study for Asia Phase III (MICS-Asia III)- Part 1: Overview and model evaluation, Atmos. Chem. Phys., 18, 4859–4884, https://doi.org/10.5194/acp-18-4859-2018, 2018.

Guo, J., Miao, Y., Zhang, Y., Liu, H., Li, Z., Zhang, W., He, J., Lou, M., Yan, Y., and Bian, L.: The climatology of planetary boundary layer height in China derived from radiosonde and reanalysis data, Atmos. Chem. Phys., 16, 13309–13319, https://doi.org/10.5194/acp-16-13309-2016, 2016.

Hu, Y. X. and Stamnes, K.: An accurate parameterization of the radiative properties of water clouds suitable for use in climate models, Journal of climate, 6, 728–742, https://doi.org/10.1175/1520-0442(1993)006<0728:AAPOTR>2.0.CO;2, 1993.

Li, D., Xue, L., Wen, L., Wang, X., Chen, T., Mellouki, A., Chen, J., and Wang, W.: Characteristics and sources of nitrous acid in an urban atmosphere of northern China: Results from 1-yr continuous observations, Atmos. Environ., 182, 296–306, https://doi.org/10.1016/j.atmosenv.2018.03.033, 2018.

Liu, X.-H., Zhang, Y., Cheng, S.-H., Xing, J., Zhang, Q., Streets, D. G., Jang, C., Wang, W.-X., and Hao, J.-M.: Understanding of regional air pollution over China using CMAQ, part I performance evaluation and seasonal variation, Atmos. Environ., 44, 2415–2426, https://doi.org/10.1016/j.atmosenv.2010.03.035, 2010.

Liu, Y., Lu, K., Li, X., Dong, H., Tan, Z., Wang, H., Zou, Q., Wu, Y., Zeng, L., and Hu, M.: A comprehensive model test of the HONO sources constrained to field measurements at rural North China Plain, Environ. Sci. Technol., 53, 3517–3525, https://doi.org/10.1021/acs.est.8b06367, 2019.

Makar, P. A., Gong, W., Milbrandt, J., Hogrefe, C., Zhang, Y., Curci, G., Žabkar, R., Im, U., Balzarini, A., Baró, R., Bianconi, R., Cheung, P., Forkel, R., Gravel, S., Hirtl, M., Honzak, L., Hou, A., Jiménez-Guerrero, P., Langer, M., Moran, M. D., Pabla, B., Pérez, J. L., Pirovano, G., San José, R., Tuccella, P., Werhahn, J., Zhang, J., and Galmarini, S.: Feedbacks between air pollution and weather, Part 1: Effects on weather, Atmos. Environ., 115, 442–469, https://doi.org/10.1016/j.atmosenv.2014.12.003, 2015.

Rasmussen, R. M., Geresdi, I., Thompson, G., Manning, K., and Karplus, E.: Freezing drizzle formation in stably stratified layer clouds: The role of radiative cooling of cloud droplets, cloud condensation nuclei, and ice initiation, Journal of the atmospheric sciences, 59, 837–860, https://doi.org/10.1175/1520-0469(2002)059<0837:FDFISS>2.0.CO;2, 2002.

Spataro, F., Ianniello, A., Esposito, G., Allegrini, I., Zhu, T., and Hu, M.: Occurrence of atmospheric nitrous acid in the urban area of Beijing (China), Sci. Total Environ., 447, 210–224, https://doi.org/10.1016/j.scitotenv.2012.12.065, 2013.

Thompson, G. and Eidhammer, T.: A study of aerosol impacts on clouds and precipitation development in a large winter cyclone, Journal of the atmospheric sciences, 71, 3636–3658, https://doi.org/10.1175/JAS-D-13-0305.1, 2014.

Tuccella, P., Menut, L., Briant, R., Deroubaix, A., Khvorostyanov, D., Mailler, S., Siour, G., and Turquety, S.: Implementation of Aerosol-Cloud Interaction within WRF-CHIMERE Online Coupled Model: Evaluation and Investigation of the Indirect Radiative Effect from Anthropogenic Emission Reduction on the Benelux Union, Atmosphere, 10, 20, https://doi.org/10.3390/atmos10010020, 2019.

Wong, D. C., Pleim, J., Mathur, R., Binkowski, F., Otte, T., Gilliam, R., Pouliot, G., Xiu, A., Young, J. O., and Kang, D.: WRF-CMAQ two-way coupled system with aerosol feedback: software development and preliminary results, Geoscientific Model Development, 5, 299–312, https://doi.org/10.5194/gmd-5-299-2012, 2012.

Xie, B., Fung, J. C. H., Chan, A., and Lau, A.: Evaluation of nonlocal and local planetary boundary layer schemes in the WRF model, J. Geophys. Res. Atmos., 117, https://doi.org/10.1029/2011JD017080, 2012.

Zhang, S., Sarwar, G., Xing, J., Chu, B., Xue, C., Sarav, A., Ding, D., Zheng, H., Mu, Y., and Duan, F.: Improving the representation of HONO chemistry in CMAQ and examining its impact on haze over China, Atmos. Chem. Phys., 21, 15809–15826, https://doi.org/10.5194/acp-21-15809-2021, 2021.

Zhao, C., Liu, X., Ruby Leung, L., and Hagos, S.: Radiative impact of mineral dust on monsoon precipitation variability over West Africa, Atmospheric Chemistry and Physics, 11, 1879–1893, https://doi.org/10.5194/acp-11-1879-2011, 2011.